The Astronomical Journal, 132:902–918, 2006 August

THE DISTRIBUTION OF THE ELEMENTS IN THE GALACTIC DISK

R. E. Luck,[1] V. V. Kovtyukh,[2] and S. M. Andrievsky[2]

Received 2006 January 20; accepted 2006 March 20

ABSTRACT

This paper reports on the spectroscopic investigation of 54 Cepheids, deriving parameters and abundances. These Cepheids extend previous samples by about 35% in number and increase the amount of the Galactic disk coverage, especially in the direction of $l \approx 120^\circ$. We find that there exists in the Galactic disk at that longitude and at a solar distance of about 3–4 kpc a region that has enhanced abundances, $\langle [Fe/H] \rangle \approx +0.2$, with respect to the local region. A simple linear fit to all Cepheid data now extant yields a gradient $d[Fe/H]/dR_G = -0.068 \pm 0.003$ dex kpc^{-1}. After consideration of the spatial abundance inhomogeneities in the sample, we conclude that the best current estimate of the overall gradient is $d[Fe/H]/dR_G = -0.06$ dex kpc^{-1}.

Key words: Cepheids — Galaxy: abundances — Galaxy: evolution — stars: abundances

Online material: machine-readable table, PDF file

1. INTRODUCTION

In previous papers from this series (Andrievsky et al. 2002a [Paper II], 2002b [Paper III], 2002c [Paper I], 2004 [Paper V]; Luck et al. 2003 [Paper IV]; Kovtyukh et al. 2005b [KWA05]) we described the characteristic features of the metallicity distribution across the Galactic disk, as derived from Cepheid variable stars. In Paper V we noted that there is an apparent steplike character in the iron (and also some other elements) abundance distribution at galactocentric distances around approximately 10–11 kpc. Twarog et al. (1997) also found such a change (discontinuity) imprinted in the metallicity distribution from open clusters. A similar conclusion has also been reached by Caputo et al. (2001) for Galactic Cepheids, although with a rather high uncertainty. Note that inward of the solar galactocentric radius the metallicity of the Cepheids increases, with the break occurring at about $R_G = 7$ kpc.

Any structure within the metallicity distribution, such as the detected steplike metallicity change, if it is proved to be real, may have some important consequences for scenarios of the formation and evolution of our Galaxy. However, before evaluating the impact of the structure in the metallicity distribution on the Galactic models, it must be proved that a slope change near $R_G \approx$ 10–11 kpc does really exist. For example, it is not impossible that such a feature could be an artificial result from a statistically limited sample of distant Cepheids, and thus may not be seen for a larger sample of stars. On the other hand, even being real, the slope change may turn out to be a purely local phenomenon that results from a possible short-scale inhomogeneity in the disk, and thus is seen in a restricted longitudinal range. It should be noted that our sample of distant Cepheids examined in Papers III–V is in fact biased on the basis of Galactic longitude, so that the great majority of investigated stars fall in the region of l from 190° to 250° (it is interesting to note that all distant open clusters investigated by Twarog et al. fall in the same general region: l from 130° to 260°). There have also been two recent investigations of the outer disk that are of interest in terms of the objectives of this work. These are the Yong et al. (2005) study of distant open clusters and, especially, the Yong et al. (2006) study of distant Cepheids.

We present here the results of the abundance determinations for 54 Galactic Cepheids, the majority of which have not been investigated spectroscopically before (at least for detailed elemental abundance determination). Eighteen of these stars fall in the region of $l \approx 120^\circ$, and thus will help relieve (or perhaps exacerbate) some of the concerns expressed in the previous paragraph. These stars have galactocentric distances placing them in the region between $R_G \approx 9$ and 11 kpc, where the feature in the metallicity distribution is seen. We also briefly explore the dependence of the derived abundances on atmospheric models and derive C and O abundances for this new sample using spectrum synthesis. The list of Cepheids considered can be found in Table 1 along with some basic data.

2. SPECTROSCOPIC MATERIAL

High signal-to-noise ratio (S/N) spectra were obtained during several observing runs between 2003 and 2005. For all observations we used the Sandiford Cassegrain Echelle Spectrograph (McCarthy et al. 1993) attached to the 2.1 m telescope at McDonald Observatory. The spectra cover a continuous wavelength range from 570 to 700 nm with a resolving power of about 60,000. Typical S/N values for the spectra are in excess of 100. Each night we observed also a broad-lined B star with a S/N exceeding that of the program stars to enable cancellation of telluric lines where necessary. Table 1 also contains details concerning our program Cepheid observations.

We used IRAF[3] to perform CCD processing, scattered light subtraction, and echelle order extraction. For all further reductions a Windows-based graphical package (ASP) developed by R. E. L. was used. This includes Beer's law removal of telluric lines, smoothing with a fast Fourier transform procedure, continuum normalization, and wavelength calibration using template spectra. Finally, equivalent widths were determined using the Gaussian approximation to the line profile (the list of the lines used in our analyses and their oscillator strengths, derived from an inverted solar analysis, are given in Kovtyukh & Andrievsky [1999]). It

[1] Department of Astronomy, Case Western Reserve University, 10900 Euclid Avenue, Cleveland, OH 44106-7215; luck@fafnir.astr.cwru.edu.

[2] Department of Astronomy, Odessa National University, Shevchenko Park, 65014 Odessa, Ukraine; scan@deneb1.odessa.ua.

[3] IRAF is distributed by the National Optical Astronomy Observatory, which is operated by the Association of Universities for Research in Astronomy, Inc., under cooperative agreement with the National Science Foundation.

TABLE 1

PROGRAM CEPHEIDS

Cepheid	Spectral Type	V (mag)	Period (days)	l (deg)	b (deg)	d (pc)	R_G (kpc)	Ref.	UT Date	UT Time	Exp.	Phase	RV (km s^{-1})	S/N	C
AN Aur	F6–F9	10.5	10.290	164.9	−1.0	3333	11.15	BI	2004 10 29	8:53	3600	0.019	−5.7	81	Y
AP Sgr	F6–G1	7.51–8.44	5.058	8.1	−2.4	822	7.09	S89	2004 08 05	4:09	900	0.093	−32.4	241	
AS Per	F8–G1	9.7	4.973	154.1	−0.9	1330	9.11	S91	2003 10 17	10:29	2700	0.580	−21.2	139	
BB Sgr	F6–G1	6.9	6.637	14.7	−9.0	826	7.11	S89	2003 10 18	1:35	600	0.878	11.5	199	
BF Oph	F6–G2	7.3	4.068	357.1	8.6	800	7.11	BI	2004 08 05	3:07	1200	0.346	−32.4	219	
BK Aur	G2	9.5	8.002	159.0	5.9	2257	10.03	G	2004 02 18	2:03	2700	0.131	−50.1	151	
BM Per	K5	10.4	22.956	155.7	−0.1	2996	10.70	BI	2004 10 29	7:44	3600	0.344	−51.4	99	Y
BZ Cyg	F8 Ib–G5 Ib	10.00–10.53	10.142	84.8	1.4	1759	7.94	S91	2004 08 07	6:25	3600	0.807	−22.0	132	
CE Cas A	F9 Ib	10.9	5.141	116.6	−1.0	2861	9.53	G	2004 08 06	10:18	3600	0.732	−63.0	75	Y
CE Cas B	F8 Ib–G0 Ib	11.1	4.479	116.6	−1.0	2979	9.61	G	2004 08 06	9:13	3600	0.153	−92.3	93	Y
CH Cas	F3p Ib–F6	11	15.087	112.9	1.6	3056	9.51	BI	2004 08 07	7:35	3600	0.108	−68.1	87	Y
CP Cep	F5 Ib–F7	10.6	17.861	100.4	1.1	4073	9.52	BI	2004 08 05	7:29	3600	0.243	−50.9	106	
CR Cep	F8	9.6	6.233	107.6	0.3	1358	8.41	G	2003 10 19	4:05	2700	0.634	−22.5	142	
CY Cas	G0 Ib–G2 Ib	11.07–12.21	14.377	113.9	2.0	3609	9.92	G	2004 10 30	3:23	3600	0.391	−87.9	63	Y
DD Cas	F7–G1	9.9	9.812	116.8	0.5	2847	9.53	S91	2004 10 30	4:33	3600	0.039	−77.4	125	Y
FM Cas	F7–G0 I	9.1	5.809	117.8	−6.3	1898	8.94	G	2003 10 17	5:40	2700	0.669	−13.5	116	
GQ Ori	G0	8.9	8.616	199.8	−4.4	2438	10.22	BI	2004 02 17	2:03	1800	0.074	29.9	150	
IR Cep	G0	7.9	2.114	103.4	4.9	521	8.04	S91	2003 10 19	3:38	900	0.385	−6.5	176	
MW Cyg	F8–G2 Ib	9.5	5.955	70.9	−0.6	1381	7.56	BI	2003 10 18	2:28	2700	0.458	−15.3	154	
RR Lac	F6–G2	8.8	6.416	105.6	−2.0	1767	8.55	BI	2003 10 18	3:36	2100	0.518	−31.4	158	
RV Sco	F5–G1	6.61–7.49	6.061	350.4	5.7	754	7.16	S89	2004 08 05	2:38	1200	0.673	−3.1	217	
RW Cas	F6–G5	9.1	14.797	129.0	−4.6	2851	9.94	BI	2004 10 29	6:34	3600	0.744	−42.9	113	Y
RY Cas	F5–G3 Ib	9.9	12.138	115.3	−3.3	2606	9.31	BI	2004 10 29	3:53	3600	0.074	−96.7	117	Y
RY Sco	F6–G2	7.51–8.44	20.316	356.5	−3.4	1185	6.72	BI	2004 08 05	3:38	1200	0.746	−2.2	157	
RZ CMa	F6	9.7	4.255	231.2	−1.1	1761	9.11	BI	2004 02 19	2:49	2700	0.575	37.8	32	Y
RZ CMa			4.255					BI	2004 10 29	11:19	3600	0.116	13.8	96	Y
SS Sct	F6–G0	8.2	3.671	25.2	−1.8	987	7.02	BI	2003 10 18	1:58	1200	0.999	−22.5	183	
SV Per	F6–G1	8.9	11.129	162.6	−1.5	2290	10.11	BI	2003 10 18	9:21	2700	0.894	−9.9	171	
SW Cas	F6–G2	9.7	5.441	109.7	−1.6	1931	8.74	G	2004 08 05	8:39	3600	0.791	−22.9	131	
SY Cas	F5–G0	9.9	4.071	118.2	−4.1	1861	8.93	BI	2004 08 05	9:49	4500	0.985	−28.1	113	
SZ Cas	F6–G4 Ib	9.9	13.621	134.8	−1.2	2099	9.50	BI	2004 10 30	7:03	3600	0.694	−47.5	114	Y
SZ Cyg	F9–G5 Ib	9.4	15.110	84.5	4.0	2386	8.03	S91	2004 08 06	5:51	3600	0.293	−17.5	201	
TX Cyg	F5–G6 Ib	8.58–10.02	14.709	84.4	−2.3	1075	7.87	BI	2004 08 06	7:02	2700	0.936	−21.9	169	
V Lac	F5–G0	8.9	4.983	106.5	−2.6	1594	8.49	BI	2003 10 18	4:21	1800	0.098	−40.5	174	
V0335 Pup		8.59–8.83	4.861	240.6	3.0	1894	8.98	F	2005 02 27	4:12	3600		37.0	135	
V0350 Sgr	F5–G2 Ib	7.5	5.154	13.8	−8.0	885	7.05	BI	2003 10 19	1:30	1200	0.468	11.2	192	
V0351 Cep	F8	9.4	2.806					S91	2003 10 20	4:18	2700	0.069	−16.8	155	
V0379 Cas	F6–G0	9	4.306	119.9	−1.9			G	2003 10 17	6:38	2700	0.740	−28.5	111	
V0379 Cas			4.306					G	2004 10 29	5:04	3600	0.515	−34.8	126	Y
V0386 Cyg	F5–G1 Ib	9.25–9.97	5.258	85.5	−4.9	998	7.88	S91	2004 08 06	8:09	2700	0.961	−18.2	164	
V0402 Cyg	G0 III	9.9	4.365	74.2	2.3	2073	7.60	G	2003 10 19	1:59	2700	0.514	−8.5	99	
V0465 Mon	G0	10.4	2.713	214.9	3.7	2569	10.11	S91	2004 02 18	3:01	3600	0.373	51.0	74	Y
V0532 Cyg	F5	9	3.283	89.0	−3.0	1039	7.95	S91	2003 10 19	2:57	1800	0.599	−12.6	138	
V0600 Aql	F6–G0	10.2	7.238	43.9	−2.6	1492	6.90	G	2003 10 20	1:33	2700	0.457	0.8	134	
V0733 Aql	F9 Ib	9.73–10.16	6.179					G	2004 08 05	6:32	2700	0.699	43.0	85	
V1154 Cyg	G2	9.2	4.926	77.2	8.8	1831	7.70	G	2004 08 05	5:37	2700	0.120	−13.3	141	
V1359 Aql	G5	8.9	3.732	38.3	−17.6	1284	6.98	G	2004 08 06	4:34	2700		−38.9	160	
VX Cyg	F5e–G2 I–II	10	20.133	82.2	−3.5	2908	8.04	BI	2003 10 20	2:30	2700	0.411	−18.4	133	
VY Cyg	F6–G1 Ib	9.6	7.857	82.9	−4.6	1774	7.88	BI	2003 10 20	3:23	2700	0.370	−16.2	153	
VZ Cyg	F5–G0	8.9	4.865	91.5	−8.5	1752	8.13	BI	2003 10 17	4:46	2700	0.365	−18.5	146	
X Lac	F6–G0	8.4	5.444	106.6	−2.5	1299	8.36	S91	2003 10 19	5:01	1200	0.328	−28.5	171	
XX Sgr	F6–G2	8.9	6.424	15.0	−1.9	1329	6.63	G	2004 08 05	4:35	1800	0.584	17.1	153	
XY Cas	F6 Ib–G2 Ib	9.9	4.502	122.7	−2.7	1749	8.97	G	2004 10 30	5:42	3600	0.603	−29.8	98	Y
Y Aur	F5–F9	9.6	3.859	166.8	4.3	1780	9.64	G	2004 02 19	1:45	2700	0.015	−7.9	103	Y
YZ Aur	F5–G2	10.3	18.193	167.3	0.9	4445	12.27	G	2004 10 29	10:00	3600	0.692	13.9	72	Y
Z Sct	F8–G4	9.6	12.902	26.8	−0.8	2722	5.61	BI	2004 08 06	3:21	3600	0.839	33.0	122	

NOTES.—Spectral type and magnitude data from the Combined General Catalog of Variable Stars (VizieR Online Data Catalog, II/250 [N. N. Samus et al., 2004], hereafter GCVS) are given, as well as various distances (d, distance from the Sun; R_G, galactocentric radius; see § 3.3). The references are the sources of the period and epoch information: BI, Berdnikov & Ignatova 2000; S89, Szabados 1989; S91, Szabados 1991; G, GCVS; F, Fernie et al. (1995). The S/N in all cases is per mean per pixel at full resolution (60,000) averaged over all orders. In the column headed "C," "Y" denotes stars whose spectra were binned to $R = 30{,}000$ before reduction. V1359 Aql is type DCEPS in the GCVS and is found in the Fernie Cepheid database. However, it is most likely an SRd variable (Berdnikov et al. 1998).

should be noted that many of our program spectra have overlapping orders, allowing one to determine two independent measurements of equivalent width for a significant fraction of the lines. As a rule, these independent measurements give results that vary by less than 5%. The equivalent widths used in the analysis are the simple average of the multiple measures. The list of line equivalent widths can be obtained from the authors by request.

It would be useful to compare equivalent widths from a variety of sources for our program stars, but Cepheids do not lend themselves to such efforts. The Cepheids would have to be at the same phase from different authors/measurers and should be from different sources (spectrographs). With respect to the stars in the current paper, such data do not exist. Equivalent width comparisons from similar data (spectrograph and measurement technique) have been published (Heiter & Luck 2003) for solar reflection spectra, and the comparisons are good, generally falling within a difference of 1% or less on the average.

3. METHODS

3.1. *Atmospheric Models, Synthesis Data, and Analysis Codes*

Atmospheric models were generated for each star (for the phase observed) using the Kurucz model atmosphere code ATLAS9. These models were derived using a microturbulent velocity of 3 km s^{-1}. At some phases Cepheids can have microturbulent velocities significantly deviating from this model value; however, our previous test calculations (see Luck et al. 2000) showed that changes of several kilometers per second in the microturbulent velocity used to compute the model atmosphere have little effect on the structure of the model. Thus, a mismatch between the derived microturbulent velocity for a specific star and the microturbulence used in the model computation at a 2–3 km s^{-1} level has an insignificant impact on the resulting elemental abundances.

The ATLAS9 models are one-dimensional (1D) LTE models with ODF line blanketing and a standard treatment of convection (using the default overshoot scale length). More sophisticated models; e.g., 2D with OS line blanketing and better element abundance mixes, are available (Gustafsson et al. 2002; the MARCS Web site). We have used these models with the final line data to derive abundances. We do this as a check on the abundance determination but use the ATLAS-derived abundances in discussions of spatial distributions of elements, as we *must* maintain consistency with previous analyses if we are to intercompare results.

We are also interested in carbon and oxygen abundances for the program stars. Syntheses of the C I 658.7 nm line, the O I 615.8 nm triplet, and the [O I] 630.0 nm line have been performed. The most recent carbon abundance determination for the Sun (Asplund et al. 2005b) adopted the same *gf*-value as used here for C I, and that analysis yielded a mean carbon abundance of 8.39 (relative to $\log \varepsilon_{\rm H} = 12$). The O I lines are problematic in abundance analyses, with only the 615.8 nm line being retained in the latest solar oxygen analysis (Asplund et al. 2004). We have synthesized the O I lines using the NIST database atomic parameters (also used by Asplund et al.). For our [O I] syntheses we have used the line data presented by Allende Prieto et al. (2001), except that we have used the experimental oscillator strength for the blending Ni I line (Johansson et al. 2003). In all of our syntheses we have assumed $[{\rm Ni/Fe}] = 0$. Note that the currently accepted value for the solar oxygen abundance is $\log \varepsilon = 8.69$ (Asplund et al. 2005).

The line analysis code was that of R. E. L., which derives from the LINES code of Sneden (1973). For the syntheses we have used a variant of the MOOG code of Sneden (1973). The analysis codes have been benchmarked against Kurucz's WIDTH and SYNTHE codes, as well the synthesis code used by S. M. A. and V. V. K., and all codes yield the same results to within expected numerical accuracy and differences due to assumptions (primarily partition functions and damping). For damping in the R. E. L. codes we preferentially use the van der Waals coefficients of Barklem et al. (2000) when available and otherwise compute from the Unsöld approximation (Unsöld 1938). Note that in supergiants van der Waals damping is not especially critical given the low particle density.

3.2. *Atmosphere Parameters: Temperatures, Gravities, and Microturbulent Velocities*

The effective temperature for each star at each pulsational phase has been determined using effective temperature relations that originated in the work of Kovtyukh & Gorlova (2000). These relations combine the effective temperature with a set of spectral line-depth ratios. The internal accuracy of the effective temperature determined in this way is rather high in the temperature range 5000–6500 K: typically 150 K or less (standard deviation or 10–20 K for the standard error; note that this method uses multiple measures [ratios], each obtained from a single observation). In Table 2 we give the standard deviation of the mean temperature and number of ratios used at each phase (observation). Note that the number of ratios in the calibration is 66 but that since we have overlapping spectra, it is possible (and probable) that the number of ratios used is larger, as the same calibration ratio can be measured in different orders. Another very important advantage of this method (or any spectroscopic method) is that it produces reddening-free $T_{\rm eff}$ estimates.

The method used for gravity and microturbulent velocity determination for a supergiant star such as these Cepheids is described in detail by Kovtyukh & Andrievsky (1999). This method determines the microturbulent velocity using Fe II lines: the dominant ionization species of iron and hence less susceptible to any NLTE effects that might be in play in supergiant atmospheres. The gravity value is found by enforcing the ionization balance condition (the mean iron abundance from Fe II lines equals the iron abundance that results from the Fe I–equivalent width relation extrapolated to zero equivalent width). Note that in these analyses we have used no lines stronger than 175 mÅ.

The final results of the determinations of $T_{\rm eff}$, $\log g$, and V_t are given in Table 2. The uncertainty in the microturbulent velocity and the gravity is more difficult to assess than the statistical error in the effective temperature. For the microturbulence a variation of ± 0.5 km s^{-1} from the adopted velocity causes a significant slope in the relation between Fe II line abundance and equivalent width. We therefore adopt ± 0.5 km s^{-1} as the uncertainty in the microturbulence. For $\log g$ we adopt ± 0.1 dex as the formal uncertainty based on the numerical result that a change in gravity at that level will result in a difference of 0.05 dex between the total iron abundances as computed from the Fe I and Fe II lines. Since we have forced an ionization balance, we do not allow a spread larger than 0.05 dex in the total abundance of iron as derived from the two ions and our uncertainty estimate of ± 0.1 dex in $\log g$.

3.3. *Distances*

For the determination of the Cepheid galactocentric distances the following standard formula was used:

$$R_G = \left[R_{G,\odot}^2 + (d \cos b)^2 - 2 R_{G,\odot} d \cos b \cos l \right]^{1/2},$$

where $R_{G,\odot}$ is the galactocentric distance of the Sun (7.9 kpc; McNamara et al. 2000), d is the heliocentric distance of the

TABLE 2

PARAMETERS FOR CEPHEIDS

Cepheid	Phase	$T_{\rm eff}$ (K)	σ (K)	N	Min. (K)	Max. (K)	$\log g$ (cm s^{-2})	V_t (km s^{-1})	$\log \varepsilon_{\rm Fe}$	[Fe/H] (dex)	σ (dex)	N
AN Aur	0.019	5775	83	125	5544	5975	1.64	4.05	7.34	−0.16	0.12	102
AP Sgr	0.093	6328	39	94	6209	6430	2.02	3.46	7.60	0.10	0.09	122
AS Per	0.580	5550	29	92	5486	5647	1.72	3.35	7.60	0.10	0.15	191
BB Sgr	0.878	5859	67	117	5708	6050	1.87	4.47	7.58	0.08	0.13	146
BF Oph	0.346	5685	31	118	5600	5800	1.88	3.15	7.50	0.00	0.08	159
BK Aur	0.131	6094	67	99	5878	6237	1.85	3.47	7.67	0.17	0.20	135
BM Per	0.344	5313	26	124	5184	5434	0.54	3.40	7.60	0.10	0.10	100
BZ Cyg	0.807	6038	101	98	5761	6275	1.92	4.18	7.69	0.19	0.21	126
CE Cas A	0.732	5817	100	105	5606	6047	1.73	3.81	7.68	0.18	0.26	108
CE Cas B	0.153	6249	70	79	6010	6429	2.40	3.47	7.72	0.22	0.23	105
CH Cas	0.108	6327	88	94	6015	6519	2.14	6.63	7.67	0.17	0.16	92
CP Cep	0.243	5152	37	72	5056	5239	0.54	3.00	7.49	−0.01	0.15	180
CR Cep	0.634	5443	75	104	5263	5623	1.33	4.02	7.44	−0.06	0.15	150
CY Cas	0.391	5369	59	110	5210	5516	0.85	3.45	7.56	0.06	0.21	126
DD Cas	0.039	5894	45	114	5759	5994	1.77	4.02	7.60	0.10	0.11	102
FM Cas	0.669	5427	51	81	5284	5571	1.00	3.37	7.41	−0.09	0.10	132
GQ Ori	0.074	6044	36	112	5917	6155	1.97	4.48	7.56	0.06	0.12	132
IR Cep	0.385	6085	52	88	5936	6190	2.05	2.85	7.61	0.11	0.12	143
MW Cyg	0.458	5525	30	120	5442	5615	1.87	3.87	7.59	0.09	0.12	179
RR Lac	0.518	5686	43	110	5588	5831	1.85	3.40	7.63	0.13	0.14	159
RV Sco	0.673	5398	26	113	5330	5455	1.57	3.55	7.60	0.10	0.12	160
RW Cas	0.744	5141	46	87	5003	5244	1.19	5.35	7.72	0.22	0.18	79
RY Cas	0.074	6179	36	103	6068	6304	2.40	6.29	7.76	0.26	0.13	102
RY Sco	0.746	5499	26	115	5414	5588	1.52	4.87	7.59	0.09	0.15	146
RZ CMa	0.575	5628	103	113	5374	5936	1.91	3.76	7.47	−0.03	0.20	118
RZ CMa	0.116	5987	55	116	5839	6172	2.04	3.43	7.47	−0.03	0.11	95
SS Sct	0.999	6300	70	109	6084	6463	2.04	3.63	7.56	0.06	0.16	111
SV Per	0.894	5755	50	112	5615	5937	1.86	4.13	7.51	0.01	0.11	153
SW Cas	0.791	5716	50	101	5604	5859	2.04	4.62	7.63	0.13	0.13	125
SY Cas	0.985	5762	62	110	5591	5918	2.10	4.26	7.54	0.04	0.13	132
SZ Cas	0.694	6146	72	103	5808	6385	1.70	4.22	7.54	0.04	0.19	93
SZ Cyg	0.293	5110	31	117	5019	5248	0.90	3.00	7.59	0.09	0.12	172
TX Cyg	0.936	6026	70	110	5814	6158	1.98	4.81	7.70	0.20	0.14	143
V Lac	0.098	6505	85	76	6314	6700	2.00	3.72	7.50	0.00	0.12	113
V335 Pup	...	6325	66	108	6137	6552	2.53	4.45	7.49	−0.01	0.10	117
V350 Sgr	0.468	5579	34	121	5483	5669	1.98	3.70	7.68	0.18	0.12	202
V351 Cep	0.069	5932	39	115	5819	6050	2.00	3.04	7.51	0.01	0.08	114
V379 Cas	0.740	6036	59	80	5881	6166	1.64	2.92	7.59	0.09	0.13	180
V379 Cas	0.515	5943	62	126	5747	6144	1.56	3.00	7.52	0.02	0.13	136
V386 Cyg	0.961	6307	100	97	6036	6528	2.54	4.65	7.61	0.11	0.15	113
V402 Cyg	0.514	5517	36	108	5412	5642	1.85	3.47	7.52	0.02	0.10	100
V465 Mon	0.373	6135	78	108	5861	6354	2.48	3.77	7.53	0.03	0.12	122
V532 Cyg	0.599	5933	74	106	5750	6126	1.75	3.02	7.46	−0.04	0.11	165
V600 Aql	0.457	5608	34	114	5522	5707	1.67	3.57	7.53	0.03	0.14	98
V733 Aql	0.699	5427	63	122	5232	5590	1.68	4.50	7.58	0.08	0.13	137
V1154 Cyg	0.120	5833	81	127	5607	6013	1.65	3.42	7.40	−0.10	0.10	157
V1359 Aql	...	4847	57	26	4644	5233	3.00	1.62	7.59	0.09	0.14	122
VX Cyg	0.411	5024	14	65	4991	5074	0.81	3.12	7.59	0.09	0.14	170
VY Cyg	0.370	5740	38	116	5629	5841	1.79	3.65	7.50	0.00	0.09	146
VZ Cyg	0.365	5662	25	113	5601	5737	1.80	3.28	7.55	0.05	0.13	173
X Lac	0.328	5891	37	108	5792	5991	1.60	3.05	7.48	−0.02	0.11	145
XX Sgr	0.584	5572	32	130	5438	5700	1.82	3.23	7.60	0.10	0.13	162
XY Cas	0.603	5539	39	99	5407	5645	1.61	3.52	7.53	0.03	0.14	119
Y Aur	0.015	6394	212	66	5830	6842	1.50	3.25	7.27	−0.23	0.17	78
YZ Aur	0.692	5326	157	68	4949	5637	0.67	4.36	7.13	−0.37	0.16	84
Z Sct	0.839	5708	68	111	5444	5908	2.00	5.01	7.79	0.29	0.14	123

NOTES.—For the effective temperature, σ is the standard deviation about the mean, and N is the number of line ratios that entered the mean. Min. and max. are the minimum and maximum individual effective temperature determinations. The quantity $\log \varepsilon_{\rm Fe}$ is the iron abundance relative to $\log \varepsilon_{\rm H} = 12$. [Fe/H] is the iron abundance relative to the Sun assuming $\log \varepsilon_{\rm Fe,\odot} = 7.50$, σ is the standard deviation about the mean abundance, and N is the number of lines used in the determination.

TABLE 3

SYNTHESIS RESULTS FOR CARBON AND OXYGEN

				C I 658.7 nm			[O I] 630.0 nm			O I	
CEPHEID	PHASE	[Fe/H] (dex)	V_M (km s^{-1})	log ε_C	[C/H]	[C/Fe]	log ε_O	[O/H]	[O/Fe]	log ε_O	C/O
AN Aur	0.019	−0.16	8	8.15	−0.24	−0.08	8.65	−0.04	0.12	8.82	0.316
AP Sgr	0.093	0.10	10	8.34	−0.05	−0.15	8.46	−0.23	−0.33	8.95	0.759
AS Per	0.580	0.10	10	8.35	−0.04	−0.14	8.75	0.06	−0.04	9.10	0.398
BB Sgr	0.878	0.08	13	8.33	−0.06	−0.14	8.56	−0.13	−0.21	8.88	0.589
BF Oph	0.346	0.00	8	8.44	0.05	0.05	8.71	0.02	0.02	9.08	0.537
BK Aur	0.131	0.17	14	8.13	−0.26	−0.43	8.65	−0.04	−0.21	8.51	0.302
BM Per	0.344	0.10	8	8.28	−0.11	−0.21	8.59	−0.10	−0.20	9.02	0.490
BZ Cyg	0.807	0.19	16	8.49	0.10	−0.09	8.95	0.26	0.07	8.87	0.347
CE Cas A	0.732	0.18	16	8.23	−0.16	−0.34	8.65	−0.04	−0.22	8.84	0.380
CE Cas B	0.153	0.22	14	8.44	0.05	−0.17	8.65	−0.04	−0.26	8.94	0.617
CH Cas	0.108	0.17	10	8.39	0.00	−0.17	8.85	0.16	−0.01	8.74	0.347
CP Cep	0.243	−0.01	10	8.00	−0.39	−0.38	8.53	−0.16	−0.15	9.00	0.295
CR Cep	0.634	−0.06	13	8.08	−0.31	−0.25	8.60	−0.09	−0.03	8.57	0.302
CY Cas	0.391	0.06	8	7.97	−0.42	−0.48	8.65	−0.04	−0.10	9.10	0.209
DD Cas	0.039	0.10	8	8.41	0.02	−0.08	8.76	0.07	−0.03	8.81	0.447
FM Cas	0.669	−0.09	11	7.94	−0.45	−0.36	8.48	−0.21	−0.12	8.72	0.288
GQ Ori	0.074	0.06	11	8.37	−0.02	−0.08	8.74	0.05	−0.01	8.96	0.427
IR Cep	0.385	0.11	10	8.19	−0.20	−0.31	8.73	0.04	−0.07	8.87	0.288
MW Cyg	0.458	0.09	10	8.30	−0.09	−0.18	8.83	0.14	0.05	9.09	0.295
RR Lac	0.518	0.13	11	8.35	−0.04	−0.17	8.95	0.26	0.13	8.81	0.251
RV Sco	0.673	0.10	10	8.26	−0.13	−0.23	8.71	0.02	−0.08	9.09	0.355
RW Cas	0.744	0.22	16	8.25	−0.14	−0.36	8.68	−0.01	−0.23	9.47	0.372
RY Cas	0.074	0.26	10	8.64	0.25	−0.01	9.00	0.31	0.05	9.17	0.437
RY Sco	0.746	0.09	12	8.43	0.04	−0.05	8.75	0.06	−0.03	8.81	0.479
RZ CMa 1	0.575	−0.03	11	8.22	−0.17	−0.14	8.80	0.11	0.14	8.62	0.263
RZ CMa 2	0.116	−0.03	8	8.31	−0.08	−0.05	8.64	−0.05	−0.02	9.07	0.468
SS Sct	0.999	0.06	14	8.07	−0.32	−0.38	8.65	−0.04	−0.10	8.81	0.263
SV Per	0.894	0.01	10	8.35	−0.04	−0.05	8.84	0.15	0.14	8.97	0.324
SW Cas	0.791	0.13	14	8.52	0.13	0.00	8.96	0.27	0.14	8.92	0.363
SY Cas	0.985	0.04	13	8.60	0.21	0.17	9.00	0.31	0.27	8.96	0.398
SZ Cas	0.694	0.04	15	8.26	−0.13	−0.17	8.75	0.06	0.02	8.82	0.324
SZ Cyg	0.293	0.09	8	8.32	−0.07	−0.16	8.79	0.10	0.01	9.35	0.339
TX Cyg	0.936	0.20	12	8.58	0.19	−0.01	8.86	0.17	−0.03	8.93	0.525
V Lac	0.098	0.00	10	8.33	−0.06	−0.06	8.86	0.17	0.17	8.77	0.295
V335 Pup	...	−0.01	8	8.45	0.06	0.07	8.82	0.13	0.14	8.90	0.427
V350 Sgr	0.468	0.18	10	8.51	0.12	−0.06	8.92	0.23	0.05	9.21	0.389
V351 Cep	0.069	0.01	9	8.33	−0.06	−0.07	8.92	0.23	0.22	8.85	0.257
V379 Cas 1	0.740	0.09	15	8.32	−0.07	−0.16	8.85	0.16	0.07	8.77	0.295
V379 Cas 2	0.515	0.02	10	8.27	−0.12	−0.14	8.66	−0.03	−0.05	8.77	0.407
V386 Cyg	0.961	0.11	12	8.51	0.12	0.01	8.63	−0.06	−0.17	9.02	0.759
V402 Cyg	0.514	0.02	10	8.21	−0.18	−0.20	8.80	0.11	0.09	9.16	0.257
V465 Mon	0.373	0.03	11	8.49	0.10	0.07	8.91	0.22	0.19	8.90	0.380
V532 Cyg	0.599	−0.04	9	8.29	−0.10	−0.06	8.72	0.03	0.07	8.99	0.372
V600 Aql	0.457	0.03	8	8.14	−0.25	−0.28	8.80	0.11	0.08	8.93	0.219
V733 Aql	0.699	0.08	11	8.32	−0.07	−0.15	8.73	0.04	−0.04	9.11	0.389
V1154 Cyg	0.120	−0.10	12	8.20	−0.19	−0.09	8.69	0.00	0.10	8.81	0.324
V1359 Aql	...	0.09	6	8.55	0.16	0.07	8.98	0.29	0.20	10.00	0.372
VX Cyg	0.411	0.09	8	8.09	−0.30	−0.39	8.86	0.17	0.08	9.37	0.170
VY Cyg	0.370	0.00	8	8.13	−0.26	−0.26	8.75	0.06	0.06	8.83	0.240
VZ Cyg	0.365	0.05	8	8.30	−0.09	−0.14	8.87	0.18	0.13	8.73	0.269
X Lac	0.328	−0.02	8	8.37	−0.02	0.00	8.79	0.10	0.12	8.81	0.380
XX Sgr	0.584	0.10	11	8.18	−0.21	−0.31	8.76	0.07	−0.03	9.03	0.263
XY Cas	0.603	0.03	10	8.15	−0.24	−0.27	8.60	−0.09	−0.12	9.03	0.355
Y Aur	0.015	−0.23	10	8.14	−0.25	−0.02	8.27	−0.42	−0.19	8.82	0.741
YZ Aur	0.692	−0.37	20	7.76	−0.63	−0.26	8.17	−0.52	−0.15	8.50	0.389
Z Sct	0.839	0.29	15	8.51	0.12	−0.17	8.85	0.16	−0.13	9.06	0.457

TABLE 4

AVERAGE ABUNDANCES [x/H] FOR Na–Cr

Cepheid	Na	Mg	Al	Si	S	Ca	Sc	Ti	V	Cr
AN Aur	0.02	−0.14	−0.01	−0.08	−0.49	−0.11	−0.17	−0.03	−0.31	−0.26
AP Sgr	0.47	0.25	0.08	0.27	−0.04	0.24	0.04	0.16	−0.04	0.19
AS Per	0.31	0.10	0.03	0.14	−0.05	0.06	0.06	0.14	−0.09	0.10
BB Sgr	0.36	...	0.15	0.14	−0.17	0.12	0.08	0.22	−0.10	0.09
BF Oph	0.22	0.10	0.06	0.12	−0.15	0.06	−0.01	0.11	−0.15	0.03
BK Aur	0.27	...	0.20	0.14	−0.04	0.25	0.01	0.32	−0.04	0.19
BM Per	0.30	0.22	0.12	0.26	−0.19	0.20	0.22	0.21	−0.28	0.11
BZ Cyg	0.38	...	0.24	0.29	−0.02	0.17	−0.05	0.14	−0.03	0.18
CE Cas A	0.56	...	0.01	0.33	−0.18	0.29	0.35	0.31	−0.16	0.29
CE Cas B	0.23	...	0.20	0.25	−0.07	0.29	0.35	0.31	0.05	...
CH Cas	0.28	...	...	0.14	−0.03	−0.04	0.12	0.15	0.01	0.02
CP Cep	0.13	0.10	0.07	0.10	−0.17	0.14	0.04	0.04	−0.12	−0.07
CR Cep	0.09	0.39	0.19	0.02	−0.23	0.02	−0.14	0.02	−0.36	−0.09
CY Cas	...	...	0.08	0.11	0.03	−0.01	0.08	−0.04	−0.27	0.01
DD Cas	0.30	0.20	0.10	0.10	−0.05	0.00	0.10	0.23	−0.10	0.01
FM Cas	0.17	0.20	0.30	0.09	−0.31	0.14	−0.08	0.11	−0.42	−0.08
GQ Ori	0.24	0.31	0.31	0.09	−0.18	−0.03	0.14	0.20	−0.07	−0.02
IR Cep	0.44	0.22	0.36	0.20	−0.10	0.22	0.01	0.29	−0.07	0.10
MW Cyg	0.15	0.08	0.18	0.06	−0.05	−0.01	0.05	0.07	−0.13	−0.03
RR Lac	0.16	...	0.24	0.12	−0.14	0.19	0.09	0.29	−0.10	0.18
RV Sco	0.18	0.11	0.27	0.15	−0.04	0.12	0.01	0.11	−0.06	0.18
RW Cas	...	...	0.05	0.13	...	0.28	0.30	0.10	−0.04	0.15
RY Cas	0.26	...	0.15	0.22	0.03	−0.07	0.22	0.30	0.19	0.09
RY Sco	0.44	0.60	0.28	0.13	0.07	0.03	0.28	0.09	−0.01	0.14
RZ CMa 1	0.22	0.32	...	0.09	−0.14	0.05	0.12	0.03	−0.15	0.04
RZ CMa 2	0.15	0.31	−0.12	0.03	−0.24	−0.01	−0.05	0.01	−0.19	−0.12
SS Sct	0.22	...	0.24	0.21	−0.12	0.18	0.02	0.05	−0.23	0.07
SV Per	0.25	0.16	0.09	0.04	−0.19	−0.05	−0.01	0.13	−0.13	−0.13
SW Cas	0.26	...	0.22	0.12	0.00	0.04	0.15	0.20	−0.01	0.18
SY Cas	0.16	0.32	0.15	0.07	0.01	0.10	0.10	0.22	−0.06	0.19
SZ Cas	0.51	...	0.17	0.28	−0.09	0.14	0.29	0.21	−0.21	0.14
SZ Cyg	0.44	0.03	0.22	0.25	0.11	0.19	0.09	0.13	0.05	0.10
TX Cyg	0.32	...	0.21	0.22	0.03	0.15	0.09	0.45	0.02	0.20
V Lac	0.19	−0.16	0.16	0.15	−0.13	0.10	−0.03	−0.02	−0.07	0.04
V335 Pup	0.13	0.11	0.11	0.07	−0.22	−0.14	0.00	0.13	−0.06	−0.04
V350 Sgr	0.23	0.19	0.32	0.13	−0.04	0.08	0.17	0.20	0.01	0.02
V351 Cep	0.27	−0.02	0.18	0.12	−0.19	0.19	0.05	0.20	−0.12	0.07
V379 Cas 1	0.18	...	0.22	0.15	−0.09	0.31	0.07	0.16	−0.21	0.02
V379 Cas 2	0.23	...	0.24	0.23	−0.13	−0.05	0.16	0.27	−0.11	−0.06
V386 Cyg	0.23	...	0.15	0.14	−0.06	0.02	0.09	0.14	−0.01	0.08
V402 Cyg	0.40	0.15	0.19	0.08	−0.14	0.12	0.07	0.08	−0.04	−0.05
V465 Mon	0.11	...	...	0.10	−0.21	−0.10	0.00	0.26	−0.15	−0.11
V532 Cyg	0.26	0.14	0.16	0.15	−0.18	0.12	−0.04	0.27	−0.13	0.06
V600 Aql	0.30	0.20	0.15	0.08	−0.22	0.06	0.11	0.07	−0.10	0.06
V733 Aql	0.19	0.22	0.08	0.09	0.03	−0.02	−0.04	0.05	−0.10	0.00
V1154 Cyg	0.11	0.53	0.09	0.04	−0.34	0.13	−0.02	0.08	−0.26	−0.05
V1359 Aql	0.24	0.17	0.21	0.12	0.24	0.18	0.21	0.20	0.20	0.16
VX Cyg	0.41	−0.16	0.13	0.18	−0.09	0.20	0.14	0.11	−0.02	0.10
VY Cyg	0.23	0.19	0.15	0.06	−0.29	0.06	0.02	0.13	−0.17	0.00
VZ Cyg	0.26	0.21	0.39	0.10	−0.11	0.03	0.14	0.14	−0.11	0.09
X Lac	0.21	0.07	0.09	0.10	−0.15	0.06	−0.03	0.18	−0.22	0.02
XX Sgr	0.27	0.34	0.34	0.11	−0.15	0.04	0.04	0.11	−0.02	0.10
XY Cas	0.45	...	0.10	0.13	−0.47	0.14	−0.10	0.14	−0.23	0.00
Y Aur	−0.06	...	−0.17	0.03	−0.27	−0.08	−0.32	−0.42	−0.36	−0.29
YZ Aur	0.21	...	−0.12	−0.25	...	−0.16	−0.70	−0.27	−0.73	−0.38
Z Sct	0.58	...	0.52	0.31	0.23	0.16	0.57	0.36	0.26	0.29

TABLE 5
AVERAGE ABUNDANCES [x/H] FOR Mn–Eu

Cepheid	Mn	Fe	Co	Ni	Cu	Zn	La	Ce	Nd	Eu
AN Aur	...	−0.16	−0.01	−0.19	0.00	0.01	...	−0.03	−0.03	−0.08
AP Sgr	...	0.10	...	0.06	...	0.17	0.02	0.05	...	0.14
AS Per	...	0.10	0.05	−0.08	0.19	0.24	0.10	0.02	0.07	0.10
BB Sgr	...	0.08	0.15	0.00	0.21	0.38	0.22	−0.09	−0.03	0.04
BF Oph	...	0.00	0.05	−0.09	0.16	0.15	0.10	0.02	−0.04	0.06
BK Aur	...	0.17	0.08	0.04	0.32	0.09	...	−0.09	0.31	0.14
BM Per	...	0.10	0.17	0.09	...	...	0.17	−0.01	−0.03	0.11
BZ Cyg	...	0.19	...	0.06	...	...	0.31	−0.07	0.15	0.12
CE Cas A	...	0.18	0.45	0.13	...	0.68	...	−0.17	−0.24	0.17
CE Cas B	...	0.22	0.40	0.11	...	0.25	...	0.30	0.30	0.42
CH Cas	...	0.17	...	0.11	...	0.18	...	0.11	0.20	0.50
CP Cep	...	−0.01	−0.07	−0.13	...	0.28	0.12	−0.12	0.03	0.00
CR Cep	...	−0.06	0.00	−0.19	0.10	...	0.14	−0.20	0.00	−0.11
CY Cas	0.15	0.06	0.05	−0.06	...	0.16	0.23	0.00	0.03	0.22
DD Cas	...	0.10	0.03	−0.06	0.62	0.24	0.09	−0.02	0.06	0.09
FM Cas	...	−0.09	−0.16	−0.15	−0.02	...	−0.01	−0.25	−0.14	−0.25
GQ Ori	...	0.06	0.11	−0.08	0.20	0.17	0.34	0.04	0.25	0.22
IR Cep	...	0.11	0.22	0.01	0.41	0.33	0.16	−0.01	0.28	0.12
MW Cyg	...	0.09	−0.05	−0.09	−0.01	...	0.15	0.04	0.13	0.06
RR Lac	...	0.13	0.02	0.00	0.18	...	0.44	0.00	0.29	0.08
RV Sco	0.12	0.10	0.11	0.01	0.17	...	0.27	0.03	0.21	0.01
RW Cas	...	0.22	0.15	0.12	...	...	...	0.00	0.11	0.23
RY Cas	...	0.26	...	0.06	...	0.24	...	0.35	0.40	0.53
RY Sco	...	0.09	0.13	0.01	0.19	...	0.45	0.05	0.24	0.26
RZ CMa 1	...	−0.03	−0.01	0.03	0.37	...	0.30	−0.04	0.26	0.09
RZ CMa 2	...	−0.03	...	−0.13	0.52	...	0.08	0.01	−0.01	0.14
SS Sct	...	0.06	...	−0.01	0.48	0.29	0.40	...	0.16	0.05
SV Per	...	0.01	−0.12	−0.15	0.02	0.04	0.28	0.11	0.16	0.17
SW Cas	0.41	0.13	−0.03	−0.03	−0.08	...	0.30	−0.12	0.16	0.15
SY Cas	...	0.04	0.31	−0.03	0.49	0.44	0.42	0.01	0.14	0.10
SZ Cas	0.62	0.04	...	0.03	...	...	...	0.00	0.32	0.28
SZ Cyg	...	0.09	0.07	0.02	0.43	0.39	0.21	0.00	0.03	0.15
TX Cyg	...	0.20	...	0.10	0.36	0.34	0.44	0.23	0.30	0.13
V Lac	...	0.00	...	−0.09	0.63	0.15	0.19	0.14	0.33	0.10
V335 Pup	...	−0.01	...	−0.12	0.22	−0.04	0.43	0.20	0.34	0.32
V350 Sgr	...	0.18	0.15	0.03	0.13	...	0.26	0.05	0.16	0.15
V351 Cep	...	0.01	−0.09	−0.05	0.20	0.23	0.15	0.03	0.15	0.08
V379 Cas 1	...	0.09	0.03	0.04	0.24	0.72	0.30	−0.21	0.12	0.13
V379 Cas 2	...	0.02	0.10	−0.03	...	0.29	0.30	0.09	0.12	0.09
V386 Cyg	...	0.11	...	−0.03	...	0.21	0.41	0.10	0.42	0.41
V402 Cyg	...	0.02	−0.06	−0.09	0.01	...	0.16	0.03	0.01	0.01
V465 Mon	...	0.03	...	−0.05	0.32	0.08	0.38	0.08	0.23	0.22
V532 Cyg	...	−0.04	−0.08	−0.09	0.36	0.38	0.09	0.00	−0.05	−0.03
V600 Aql	...	0.03	−0.08	−0.09	0.20	...	0.15	−0.05	0.03	0.00
V733 Aql	0.08	0.08	−0.03	−0.06	−0.08	...	0.21	−0.13	0.02	−0.08
V1154 Cyg	...	−0.10	0.05	−0.12	0.13	0.14	0.18	−0.10	0.05	−0.06
V1359 Aql	0.16	0.09	0.18	0.08	...	...	0.21	0.14	0.16	0.28
VX Cyg	...	0.09	0.11	0.04	...	...	0.16	−0.01	0.01	0.17
VY Cyg	...	0.00	−0.10	−0.11	0.09	0.10	0.21	0.01	0.09	0.01
VZ Cyg	...	0.05	−0.06	−0.07	0.13	...	0.14	0.01	0.08	0.11
X Lac	...	−0.02	0.00	−0.10	0.24	0.12	0.19	0.00	0.14	−0.02
XX Sgr	...	0.10	0.10	−0.02	0.21	...	0.43	0.10	0.27	0.09
XY Cas	...	0.03	−0.05	−0.07	0.28	...	0.16	−0.19	−0.08	−0.09
Y Aur	...	−0.23	...	−0.34	...	...	−0.22	−0.27	−0.07	−0.15
YZ Aur	...	−0.37	...	−0.32	...	...	...	−0.49	−0.26	−0.33
Z Sct	...	0.29	0.28	0.24	0.38	...	0.24	0.03	0.14	0.29

Cepheid, and l and b are the Galactic longitude and latitude, respectively. To obtain the heliocentric distances we used $d = 10^{-0.2(M_V - \langle V \rangle - 5 + A_V)}$, and to obtain A_V we used the Laney & Stobie (1993) relation,

$$A_V = [3.07 + 0.28(B - V)_0 + 0.04E(B - V)]E(B - V),$$

where M_V is the absolute magnitude, $\langle V \rangle$ is the mean visual magnitude, and A_V is the line-of-sight extinction.

To estimate the absolute magnitude we used the absolute magnitude–pulsational period relation of Gieren et al. (1998). Other input data needed for the distance such as Galactic coordinates, pulsational periods, mean visual magnitudes, colors, and $E(B - V)$

TABLE 6
DETAILED [x/H] DATA FOR PROGRAM CEPHEIDS

	AN AUR			AP SGR			AS PER			BB SGR		
ION	[x/H]	σ	N	[x/H]	σ	N	[x/H]	σ	N	[x/H]	σ	N
Na I	0.02	...	1	0.47	0.09	3	0.31	0.02	2	0.36	0.02	3
Mg I	−0.14	...	1	0.25	...	1	0.10	0.06	2	...	...	...
Al I	−0.01	0.06	2	0.08	...	1	0.03	...	1	0.15	0.06	2
Si I	−0.08	0.12	17	0.27	0.07	20	0.14	0.11	23	0.14	0.09	19
Si II	−0.09	0.06	2	...	...	...	0.07	...	1	...	...	...

NOTES.—Table 6 is published in its entirety in the electronic edition of the *Astronomical Journal*. It is also available for download as a PDF. A portion is shown here for guidance regarding its form and content.

values were taken from Fernie et al. (1995). Galactocentric distances for the program stars are listed in Table 1.

4. RESULTS

4.1. *Elemental Abundances*

The elemental abundances in our program stars are available in Table 3 (carbon and oxygen from syntheses), Tables 4 and 5 (mean [x/H] ratios for each star), and Table 6 (full table only available online; detailed abundances per star per species [$Z > 10$]). Iron abundance details (specifically Fe I) are given in Table 2 along with the stellar parameters.

4.1.1. *Internal Comparison of Parameters, Abundances, and Models*

Abundance reliability in Cepheids as a function of phase has been addressed in a recent series of papers (Fry & Carney 1997; Luck & Andrievsky 2004; Kovtyukh et al. 2005a; Andrievsky et al. 2005). Our finding is that accurate parameters and [Fe/H] ratios can be derived at any phase in a Cepheid independent of the period of the Cepheid. Based on this we would not expect any untoward effects in the abundances due to phase (stellar) parameter problems.

While there are no totally independent determinations of parameters and abundances available for these Cepheids, we have made several checks on the derived parameters and abundances. First, published abundances (by us) are available for six of these stars: three in Papers I–V and three in KWA05. The mean difference in the sense of this work compared to the previous is +0.06 for [Fe/H] for both sets of previous data. For 11 of these stars an independent spectrum reduction and abundance analysis was undertaken (by V. V. K.) in Odessa. All parameters and abundances reported here are by R. E. L. The differences (R. E. L. − V. V. K.) are +17 K in $T_{\rm eff}$, −0.03 in log g, −0.34 in V_t, and +0.05 in [Fe/H]. This represents good agreement for these stars.

We have also investigated the dependence of our abundances for these stars on the choice of model atmosphere. Gustafsson et al. (2002) have presented a new generation of MARCS models (spherical, LTE, and opacity sampling) and have made available a large selection for download on their Web site.[4] We have used the solar-metallicity CN-processed grid to interpolate models with the final derived parameters presented in Table 2. We show in Figure 1 the differences (compared to effective temperature) of MARCS (Fe I − Fe II), Fe I (ATLAS − MARCS), and Fe II (ATLAS − MARCS). We see that for our parameters the MARCS models are marginally out of ionization equilibrium [mean (Fe I − Fe II) ≈ −0.05] independent of effective temperature. This could be rectified by a systematic log g shift of −0.1 dex. The differences ATLAS − MARCS are slightly dependent on effective temperature: the difference in Fe I implied total abundance decreases from about 0.12 dex at 6000 K to about 0.06 dex at 5000 K. If the gravities of the MARCS models were decreased to give ionization equilibrium, the difference in total iron abundance would be about +0.1 (in the sense of ATLAS − MARCS). Note that the Fe I abundances would remain essentially constant, as gravity shifts in this regime primarily affect Fe II. What is perhaps more interesting relative to the model differences is the abrupt difference in the behavior of Fe I at about 5250 K in the MARCS models. It appears that at this temperature there is a major change in the models most likely due to differences in the neutral-to-ionized ratios changing at different effective temperatures in the two model types, (especially) due to differing assumptions about geometry.

Two further comments about the use of MARCS models are warranted. First, a caveat about the choice of model parameters. The effective temperature used here is that derived from the Kovtyukh & Gorlova (2000) calibration. That calibration depends on previous effective temperature determinations that may or may not be consistent with the new MARCS models. Second, in order to maintain consistency in the derivation of spatial abundance distributions we *must* use the same models as used in our previous work; e.g., ATLAS models.

4.1.2. *Comparison with Yong et al. (2006)*

Yong et al. (2006) give abundances for 25 distant Cepheids and a further 11 "nearby" Cepheids. Only one of these stars (YZ Aur) is included here. However, all of the nearby Cepheids

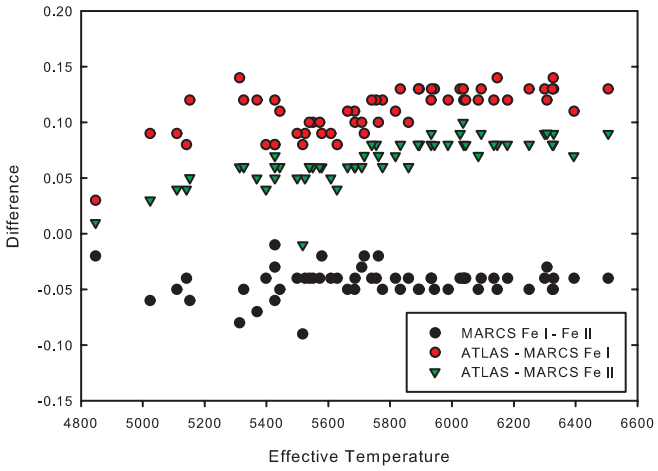

FIG. 1.—Comparison of iron data as derived from Fe I and Fe II for ATLAS9 and the new MARCS models (Gustafsson et al. 2002). See text for discussion.

[4] See http://marcs.astro.uu.se.

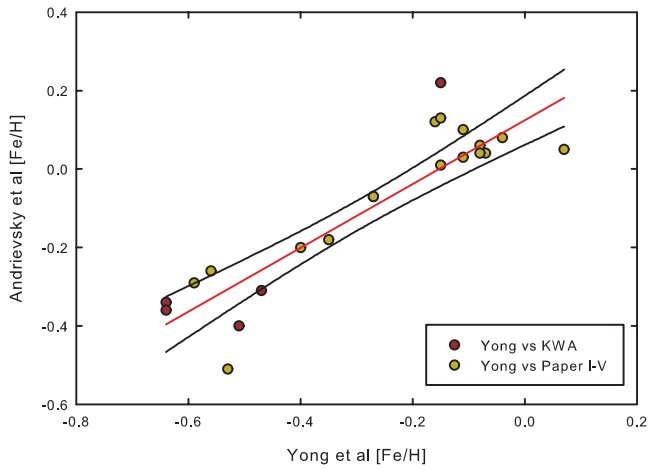

FIG. 2.—[Fe/H] data from Papers I–V and KWA05 vs. the [Fe/H] results of Yong et al. (2006). The mean offset is about 0.18 dex, with our values being the larger.

and nine of the distant Cepheids of Yong et al. are included in Papers I–V and/or KWA05. In Figure 2 we show the comparison of [Fe/H] ratios (we show only the KWA05 value for YZ Aur; the value derived here is different by only 0.05 dex). It is obvious that our work is on a higher abundance scale than the values presented by Yong et al. The difference is mainly an offset, but there is a slight dependence on [Fe/H] itself:

$$[\mathrm{Fe/H}]_{\mathrm{Yong}} = -0.175(\pm 0.0243) + 1.036(\pm 0.106)[\mathrm{Fe/H}]_{\mathrm{us}}$$
$$(n = 20, \quad \sigma = 0.094),$$

where $[\mathrm{Fe/H}]_{\mathrm{us}}$ refers to Papers I–V combined with KWA05.

What gives rise to the offset in [Fe/H]? The obvious candidates are the stellar parameters: effective temperature, surface gravity, and microturbulence. Yong et al. used a traditional spectroscopic approach to the determination of these values: an excitation analysis for effective temperature, an ionization balance for gravity, and demanding no dependence of individual line abundances of Fe I on line equivalent width. We use effective temperatures derived from line ratios, determine the microturbulence from the dominant ionization stage Fe II, and then perform an ionization balance by extending the Fe I–equivalent width relation to 0 eV and forcing that iron abundance to be equal to the Fe II value. The question is: How do the derived parameters compare?

We begin with effective temperature. The original Kovtyukh & Gorlova (2000) calibration depended on the excitation temperature analysis of Fry & Carney (1997) combined with the photometric results of Kiss & Szatmary (1998). The current calibration uses the previous information combined with the excitation analysis results for supergiants of Luck & Bond (1989) and the 13 color photometry results of Bravo Alfaro et al. (1997). Luck & Bond showed that their effective temperatures were consistent with the $V - K$ calibration of Ridgway et al. (1980) and agreed well with their $J - K$ calibration, especially at temperatures above 4600 K. Contrary to the statement of Yong et al. (2006), our method is *not* totally dependent on previous excitation analyses. More importantly, it has been demonstrated to yield consistent results as a function of phase for numerous Cepheids spanning periods from 3 to 47 days (Luck & Andrievsky 2004; Kovtyukh et al. 2005a; Andrievsky et al. 2005). Yong et al. published phase data for their nearby Cepheids, and a comparison

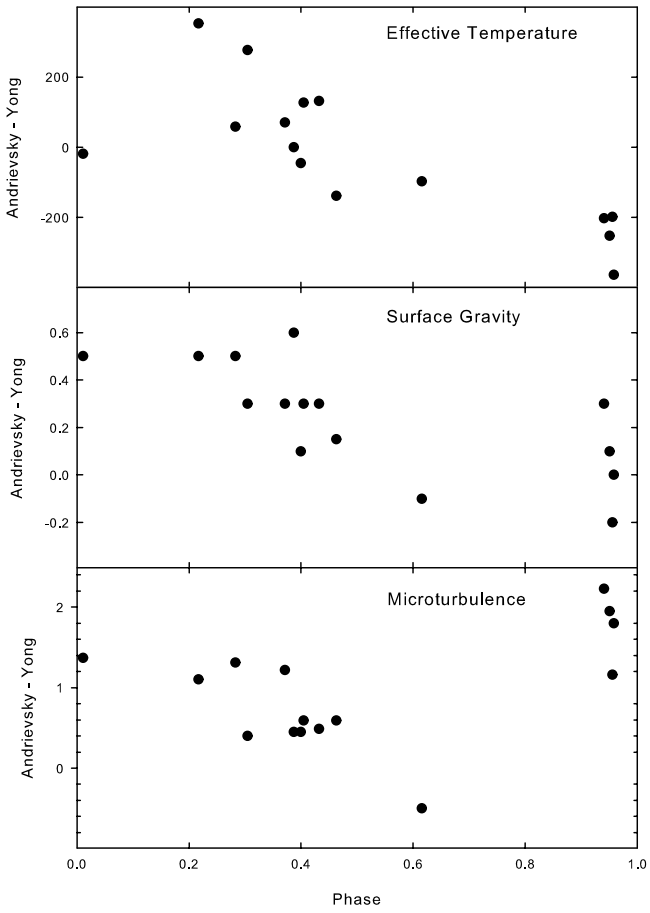

FIG. 3.—Comparison of the differences in the phase-dependent parameters of effective temperature, log g, and V_t in the sense of Andrievsky et al. (Papers I–V; KWA05) compared to Yong et al. (2006). There appears to be a phase-related difference in each parameter.

of temperature differences with respect to our phase-dependent data yields a scatter diagram (the same is true of gravity and microturbulence). Note that while we cannot always match phase exactly, we can always find corresponding data to within about 0.05 in phase in our data. However, if we plot the differences (see Fig. 3, *top*) we find that there is a strong phase effect in the differences: our effective temperatures are higher than the Yong et al. values during descending light (phase 0 to about 0.35) and lower during ascending light (about phase 0.65 to 1.0).

Yong et al. (2006) indicate that their gravities are systematically low with respect to the Fernie (1995) log P–log g relation by about 0.19 dex. We show in Figure 4 the relation between the gravities of the stars of this study and log P. The Fernie relation is also shown; our stars average 0.05 dex higher in log g than the Fernie relation and have a scatter with respect to that relation, as expected based on our phase-dependent values. The implication is that our log g values should average about 0.24 dex higher than the Yong et al. values, and this indeed is what is found when we examine the nearby Cepheid data of Yong et al. versus our previous phase-dependent data. As before, there is a phase dependence in the differences (see Fig. 3, *middle*). Note that from integration of the radial velocity curve we get the radius curve, but not the acceleration terms. The instantaneous gravity value (i.e., the measured gravity) depends on not only the current radius value but also on the dynamical term $\gamma^* dV_r/dt$. Luck et al. (2001) give a comparison of the measured gravities of SV Vul with dynamical gravities.

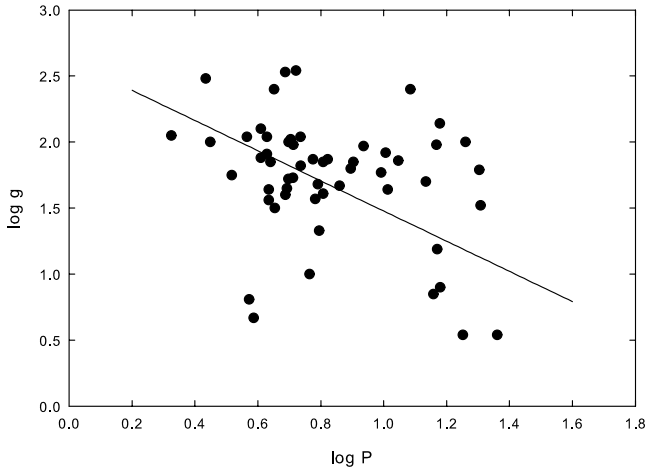

FIG. 4.—The log g values of this work vs. the Fernie (1995) log P–log g relation. The mean difference is +0.05 (our gravities are higher), with no discernible dependence on period. The scatter is consistent with the gravity amplitudes found in phase-dependent studies.

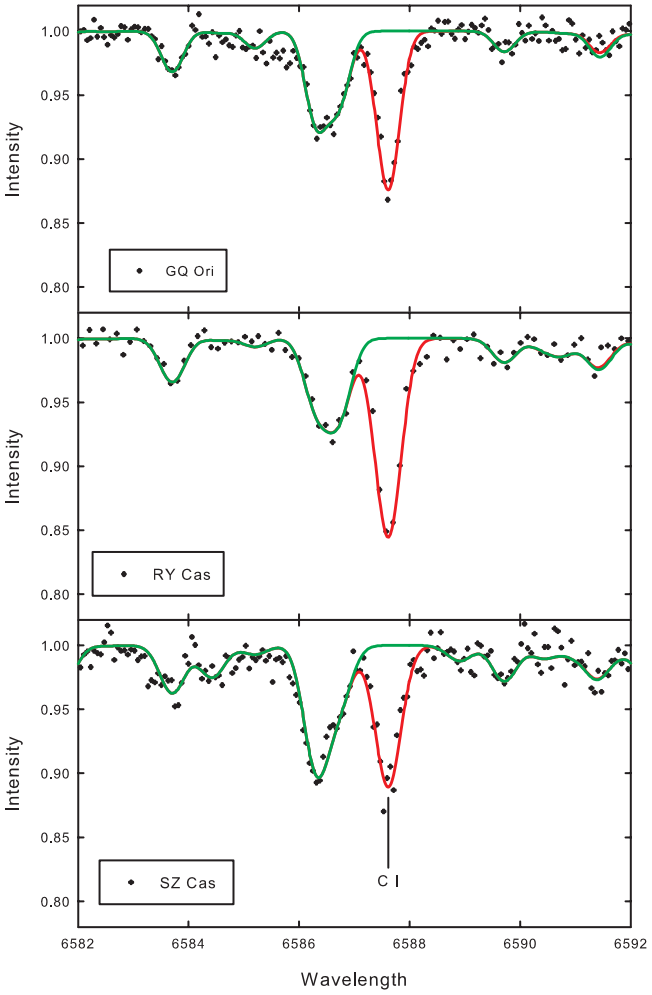

FIG. 5.—Syntheses of C I 658.7 nm in three Cepheids. The green synthesis includes the C I line, while the red line does not. There is no ambiguity about the presence or strength of the line in Cepheid variables.

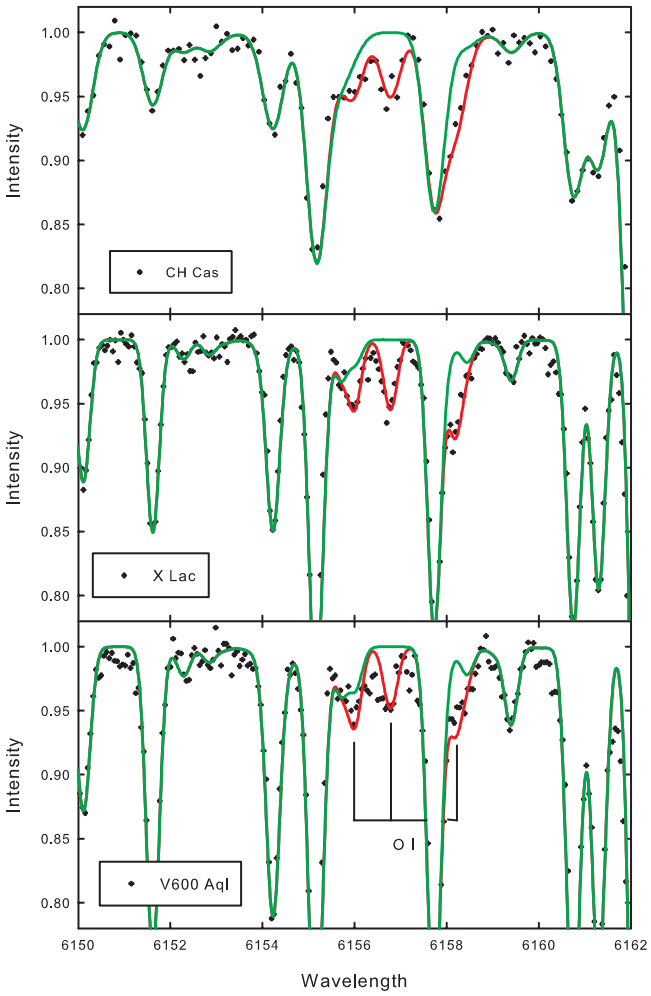

FIG. 6.—Syntheses of O I 615.7 nm in three Cepheids. The green synthesis includes the O I lines, while the red line does not. Where the triplet is present it is blended with other features.

As a last point, Figure 3 (*bottom*) shows the microturbulent velocity comparison. As with the temperature and gravity there appears to be a phase dependence in the differences. We believe the combination of the various phase-dependent differences in the Yong et al. (2006) data relative to ours is the source of the systematic [Fe/H] difference. Why would there be a phase-dependent difference in these two analyses? Truthfully, we are at a loss to explain it. We reiterate, however: our methods have been demonstrated to yield consistent results as a function of phase for numerous Cepheids.

4.1.3. *Synthesis Results*

Table 3 gives the synthesis results for the abundances of carbon and oxygen for the program stars. The quoted abundances take into account the interlocking of the carbon and oxygen abundance due to the CO molecule (although the effect is minimal at these parameters and abundance levels). Representative syntheses are presented in Figures 5–7. As can be seen, the C I 658.7 nm and [O I] 630.0 nm lines are of moderate strength, yielding good abundances. The O I 615.7 nm triplet is heavily blended, and while of reasonable strength does not yield an abundance of the quality as determined from the forbidden line. Our estimate of the accuracy of the carbon and oxygen abundances is ± 0.1 dex based on trial syntheses.

From the data presented in Table 3 it is clear that there exists a scale problem in the oxygen abundances as determined from

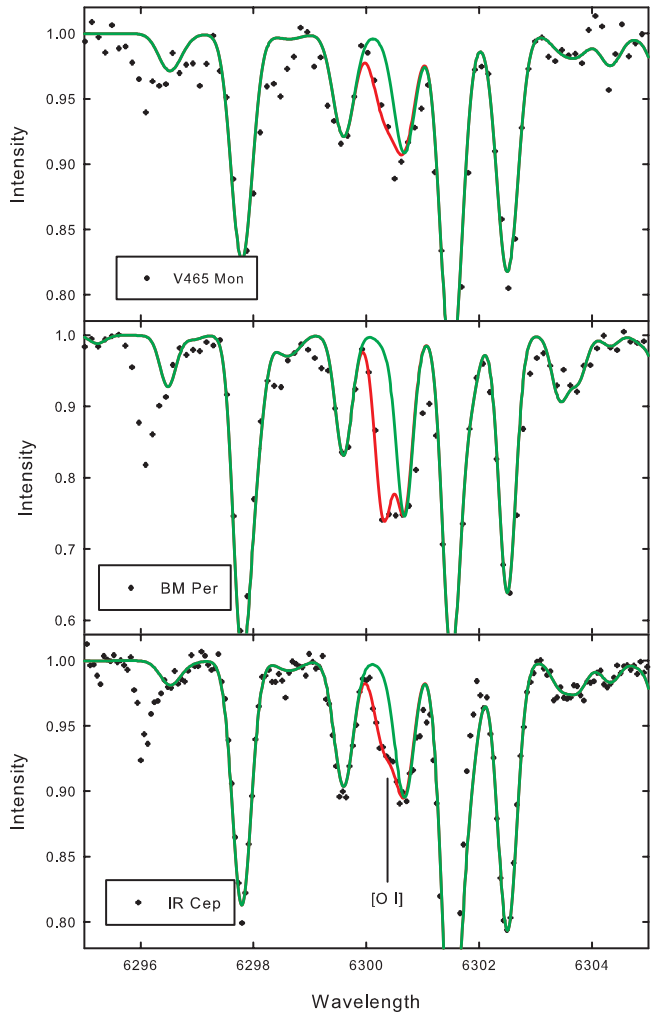

FIG. 7.—Syntheses of [O I] 630.0 nm in three Cepheids. The green synthesis includes the [O I] line, while the red line does not. There is no ambiguity about the presence or strength of the line in Cepheid variables.

[O I] and O I. The mean log ε_O for [O I] is 8.74 (very close to the currently accepted solar value of 8.69), while for O I we obtain 8.95. This difference is not likely due to *gf*-value problems; both indicators use the best current values as adopted by solar analyses (Asplund et al. 2004). The O I triplet shows no obvious trends with temperature or gravity. We thus consider the O I 615.8 nm triplet problematic at best, and we do not consider it further in our discussion.

The [Fe/H] ratios in the current sample span a range of 0.7 dex, and we expect and find a similar span in the carbon and oxygen abundances; the observed span for both carbon and oxygen is about 0.9. For these stars the mean [C/Fe] ratio is -0.15 ($\sigma = 0.14$, and $n = 56$; we have retained separate abundances for the two stars with two phases), while the mean [O/Fe] ratio is 0.00 ($\sigma = 0.14$). These mean ratios are about as expected based on standard stellar evolution models for stars of this mass after the first dredge-up (Iben 1966a, 1966b, 1966c; Schaller et al. 1992; Girardi et al. 2000): oxygen is not modified, and carbon is diluted relative to the original content. Unfortunately, we have no data on nitrogen, which is expected to increase in abundance.

We have examined the behavior of carbon and oxygen as a function of parameters and abundance. We show in Figure 8 (*top*) carbon, oxygen, and iron versus log *P* (effectively mass), as well as [C/Fe] and [O/Fe] (Fig. 8, *bottom*). All of the trend information

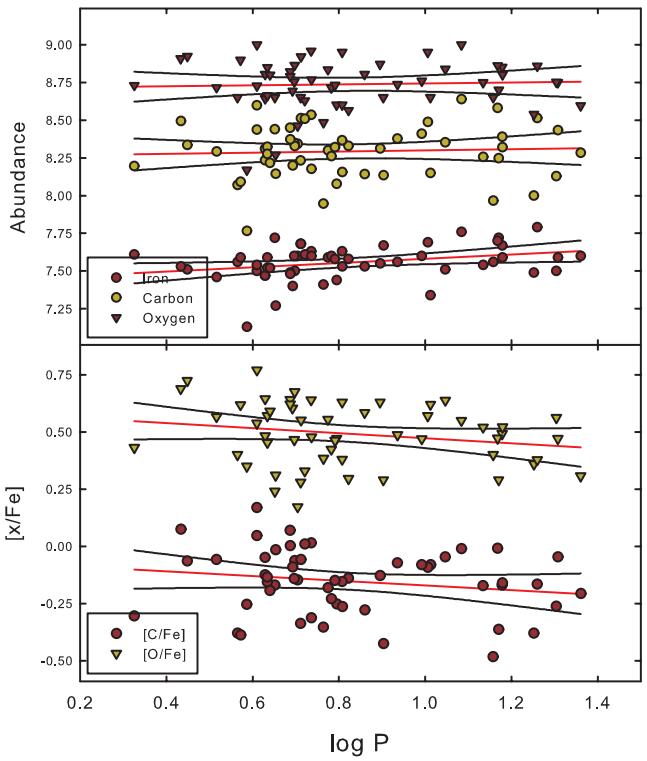

FIG. 8.—[C/Fe] and [O/Fe] vs. log *P* for the program stars. There is no significant trend apparent in the data. Note that the [O/Fe] data have been shifted by +0.5 to separate them from the [C/Fe] data.

is consistent with no correlation between period (and thus mass) and the abundances or abundance ratios.

Figure 9 shows the behavior of carbon versus oxygen. The abundances are correlated with a correlation coefficient of 0.68 (Pearson product moment correlation), and [O/H]-[C/H] and [C/Fe]-[O/Fe] show a similar correlation (correlation coefficient of $\approx$0.58). However, Smiljanic et al. (2006) have interpreted their CNO abundances in intermediate-mass stars as implying no correlation. We feel that the correlation observed here reflects the original composition and the effects across the mass range of these stars of the first dredge-up.

Before continuing we would like to point out a last item concerning the oxygen abundances derived here. Our mean oxygen

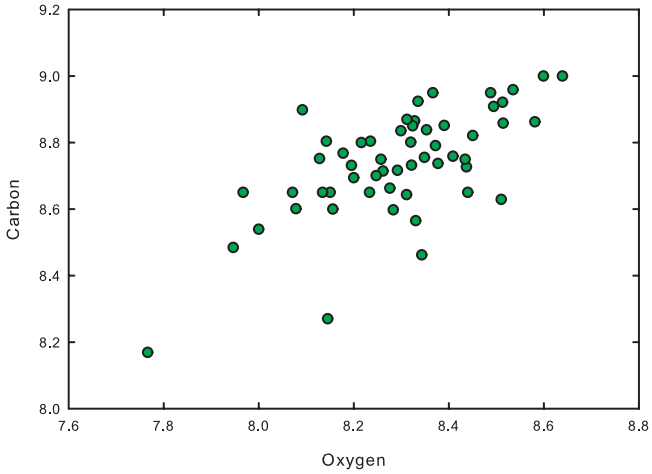

FIG. 9.—Carbon vs. oxygen for the program Cepheids. The abundances are correlated, reflecting original composition and comparable evolutionary effects.

abundance is 8.74 ($\log \varepsilon_{\rm O}$) and the mean [O/Fe] ratio is 0.00. The quoted ratios ([O/H] and [O/Fe]) for these Cepheids use (assume) the most recent determination of the solar oxygen content. The oxygen abundance determined for Cepheids here is consistent with previous oxygen abundances in intermediate-mass stars (which include Cepheids, nonvariable supergiants, and their progenitor B stars), starting with Luck (1978) and proceeding through Smiljanic et al. (2006). What is different is that now the imputed [O/H] ratio is +0.05, not −0.2. The intermediate-mass abundances have not changed, but the best current estimate of the solar abundance of oxygen has. The current value is 8.69 (Asplund et al. 2005), not the previously used 8.92. At first consideration the solar abundance of oxygen is now in good agreement with that found in intermediate-mass stars. However, this is most probably not the last word on the subject. The difficulty is that the new solar oxygen value is mostly due to the use of a 3D model in the analysis, while the Cepheid oxygen abundances still rest on 1D models.

We have investigated a variety of 1D solar models with the new synthesis data ([O I] revised *gf*-value and the Ni I line) coupled with a solar flux spectrum (obtained with the same observing setup used for the Cepheids and using Callisto as a mixer/reflector for the solar spectrum). We have used a MARCS75 model (Gustafsson et al. 1975), the MARCS2002 model (Gustafsson et al. 2002), an ATLAS9 model, the Holweger (1974) semiempirical model, and finally, the Grevesse & Sauval (1999) revised semiempirical model to derive the solar oxygen content. We find $\log \varepsilon_{\rm O}$ to be 8.74, 8.81, 8.84, 8.88, and 8.84, respectively, for these models. As can be seen, these values are more akin to the older solar value of $\log \varepsilon_{\rm O} = 8.92$, which if used would yield a Cepheid/supergiant [O/H] ratio of −0.18, as previously found. In our abundance tables we give [O/H] computed using a solar oxygen abundance of 8.69 but do not assign any specific importance to the chosen zero point. It appears that the oxygen abundance problem in intermediate-mass stars persists.

4.2. *Spatial Abundance Distributions*

4.2.1. [Fe/H] *Distribution*

Based on Tables 2–5, and the results of Papers I–V, KWA05, and Yong et al. (2006), we have constructed radial (1D) distributions of elemental abundances. From the Yong et al. data we use the 15 stars in that study that are not included in our studies. We have placed their [Fe/H] data on our scale using the transformation given in § 4.1.2 and shown in Figure 2. Distances for the Yong et al. stars have been derived using the formalism of § 3.3. The galactocentric distances are comparable to those of Yong et al. with the glaring exception of HQ Car, for which the derived distance from the $\langle V \rangle$ and M_V data is 12.4 kpc, while the $(\langle K \rangle, M_K)$ data used by Yong et al. yield 15.7 kpc. In Figure 10 we show the gradient data for iron.

If we divide the whole range into three parts (zone I: 4.0–6.6 kpc; zone II: 6.6–10.6 kpc; and zone III: 10.6–14.6 kpc), then the statistics for each zone and the total sample for iron (the most reliable abundance) are as follows: for zone I,

$$[\mathrm{Fe/H}] = -0.128(\pm 0.050) R_G + 0.936(\pm 0.293),$$
$$\langle [\mathrm{Fe/H}] \rangle = +0.182 \quad (\mathrm{s.d.} = 0.128, \quad n = 13),$$

for zone II,

$$[\mathrm{Fe/H}] = -0.026(\pm 0.007) R_G + 0.236(\pm 0.061),$$
$$\langle [\mathrm{Fe/H}] \rangle = +0.015 \quad (\mathrm{s.d.} = 0.093, \quad n = 141),$$

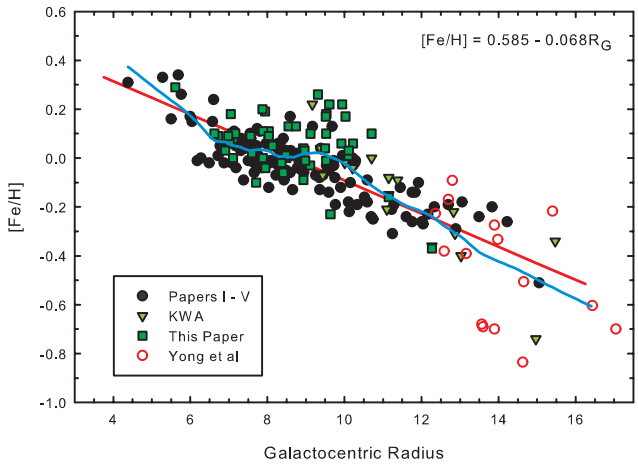

FIG. 10.—[Fe/H] vs. galactocentric distance for the complete sample of Cepheids, including the stars of Yong et al. (2006) not found in our work. The linear fit has a slope $d[\mathrm{Fe/H}]/dR_G = -0.068$ dex kpc^{-1}. The blue line is a LOWESS local smoothing fit. See § 4.2 for more discussion.

for zone III,

$$[\mathrm{Fe/H}] = -0.090(\pm 0.013) R_G + 0.849(\pm 0.173),$$
$$\langle [\mathrm{Fe/H}] \rangle = -0.297 \quad (\mathrm{s.d.} = 0.200, \quad n = 51),$$

and for the total,

$$[\mathrm{Fe/H}] = -0.068(\pm 0.003) R_G + 0.585(\pm 0.033).$$

As one can see, the mean metallicities for these zones are different. The mean metallicity of zone II is heavily influenced by the group of higher abundance stars at galactocentric radius $R_G \sim 9$–10 kpc, while in zone III the low-abundance stars at about 14 kpc have a similar influence. Without those stars the slope would be essentially constant across zones II and III. The difference in the slopes and mean metallicities across the disk are traced in the plots for all elements through the iron peak.

The linear gradient that we have derived here is $d[\mathrm{Fe/H}]/dR_G = -0.068$ dex kpc^{-1} for the total sample. If one uses our data exclusively, one obtains a gradient of −0.059 dex kpc^{-1}. The addition of the lower abundance stars of Yong et al. (2006) has a significant influence on the gradient value. There have been many attempts to determine the value of the gradient (see Paper I for a brief history). The value derived here is somewhat higher than the recent value from Maciel et al. (2005) of $d[\mathrm{Fe/H}]/dR_G = -0.054$ dex kpc^{-1} (based on our previous Cepheid abundances and a somewhat revised distance scale). L. Chen & J. L. Hou[5] derived $d[\mathrm{Fe/H}]/dR_G = -0.063$ dex kpc^{-1} from a sample of young open clusters. These values are also in accord with the somewhat older results of Friel (1999) and Phelps (2000), who obtained $d[\mathrm{Fe/H}]/dR_G = -0.06$ dex kpc^{-1}.

In previous papers we have smoothed the [Fe/H]-R_G relation by use of a local smoothing method (LOWESS, in particular). Figure 10 includes the result of such a smoothing. As can be seen, the smoothed fit is not significantly different from the linear fit, especially at galactocentric distances greater than about 7 kpc. Interior to that radius there is an increase in the slope, but that region is sampled only by 13 stars (relative to the 205 in the

[5] See http://www.rssd.esa.int/index.php?project=Gaia&page=Gaia_2004_Proceedings.

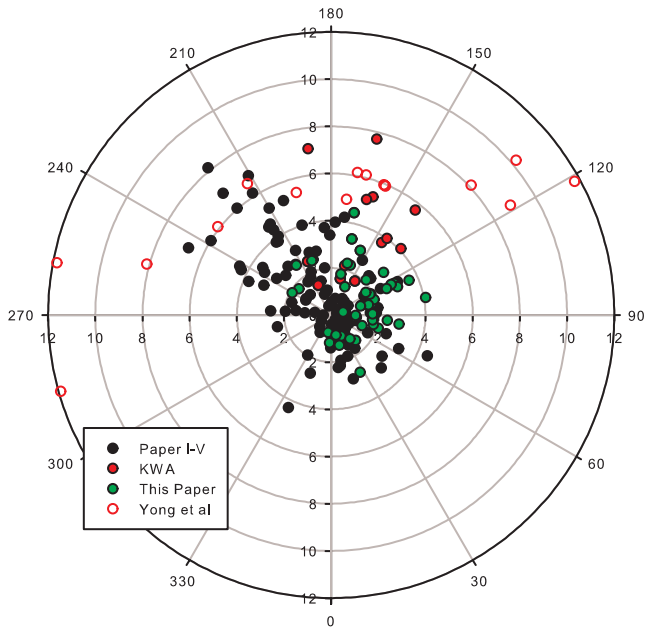

FIG. 11.—Galactic longitude (l)–distance from the Sun (d) distribution of the current Cepheid samples available for spatial abundance distribution analysis.

total sample). It is also apparent that the behavior of the local smoothing in the region of 9–10 kpc is heavily influenced by the knot of higher abundance stars at that radius. Our previous work had four higher abundance stars in this radius range, but this study has more than doubled that number.

In Figure 11 we show the spatial distribution of the total sample in Galactic longitude (l) and distance from the Sun (d). As one would expect, the density of observed stars decreases as the distance from the Sun increases. The reason is twofold: first, distant stars require the investment of significant observing time; and second, as one approaches the edge of the Galaxy ($R_G \approx 16$ kpc or $d \approx 8$ kpc from the Sun toward $l = 180^\circ$) the stellar density decreases. Note that the extent of the stellar disk of the Milky Way is rather uncertain. The stellar scale length is somewhere around 3 kpc for the Milky Way (Zheng et al. 2001; López-Corredoira et al. 2002), which implies a stellar disk of about 12 kpc based on external spirals (de Grijs et al. 2001). López-Corredoira et al., however, find no indication of a cutoff in the Galactic stellar disk at radii $R_G < 15$ kpc. In addition, there is evidence of spiral structure at R_G from 18 to 24 kpc (McClure-Griffiths et al. 2004). Thus, it is possible that the Cepheids thus far sampled do not approach the full radius of the Milky Way. One of the goals of the present study was to increase the longitudinal coverage of our sample, and we have made a start on this: the current sample is primarily in the $l = 0^\circ$–180° range at distances greater than 1 kpc from the Sun, where our previous sample had a paucity of stars. Of particular interest is the group of stars at $l \approx 120^\circ$ at about 3 kpc from the Sun. Note that the Yong et al. (2006) data have another group of stars at a larger distance from the Sun in the same direction.

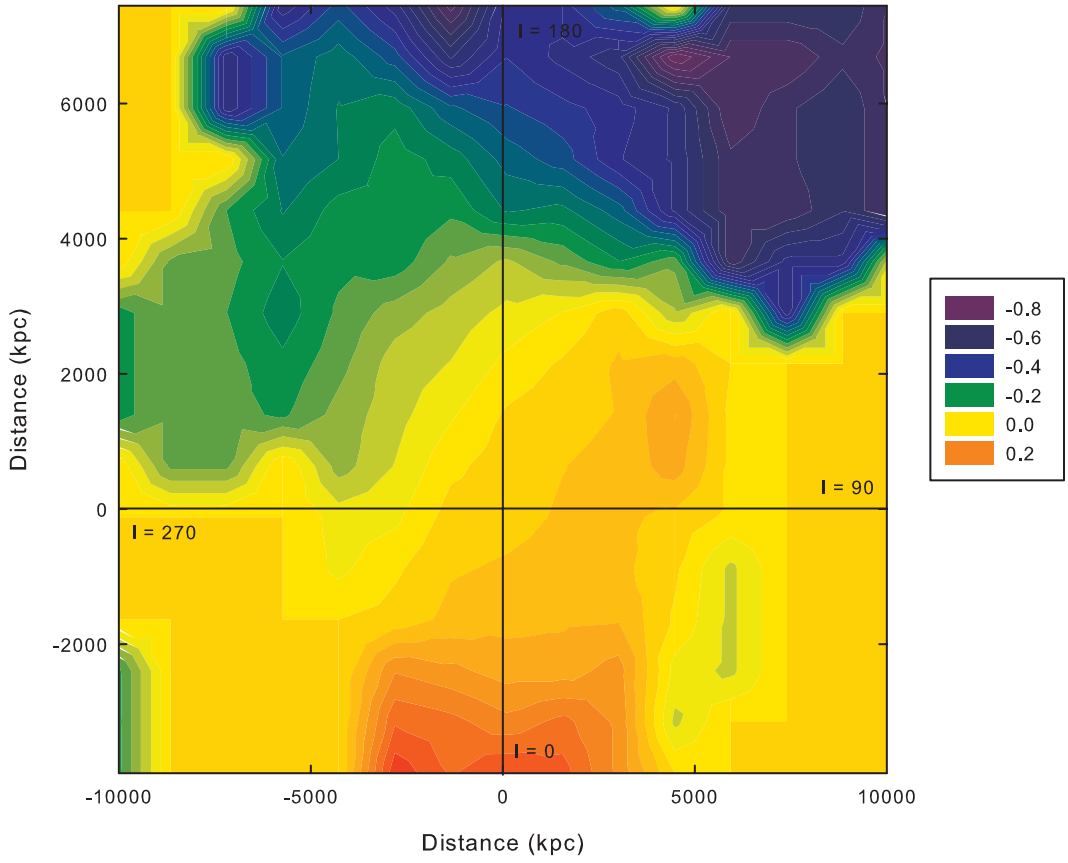

FIG. 12.—Contour map of the [Fe/H] ratio vs. spatial position. The Sun is located at the intersection of the two fiducial lines at $(x, y) = (0, 0)$ kpc. Note the presence of the high-abundance area at $(x, y) \approx (2, 2)$ kpc, which is at $(l, d) \approx (120^\circ, 3$–$4$ kpc).

The knot of high-abundance stars at $R_G \approx 9.5$–10 kpc is strongly influenced by the new stars of this sample. We were curious as to the spatial distribution of these stars, and to investigate this we have created a surface map of the iron abundance as given by the Cepheid data. This is shown in Figure 12. The Sun is at (0, 0) in the plot. Note the increase of abundance toward the Galactic center (0, −7900) and the general decrease in abundance toward the outer regions of the Galaxy. The most interesting feature of the surface map is the localized high-abundance region at $l \approx 120^\circ$ at about 3–4 kpc from the Sun. These are the stars that comprise the bulk of the high-abundance stars in the radial gradient plot at $R_G \approx 9.5$–10 kpc. This means that the annulus at $R_G \approx 9.5$–10 kpc is not homogenous; there is a local structure in it about 3 kpc from the solar system. This region is enhanced in abundance by about +0.2 dex relative to the solar region. *This is the first evidence from these studies that the Galaxy has localized abundance inhomogeneities most likely due to "recent" supernovae [SNe] events.*

What are the characteristics of the region at $l \approx 120^\circ$ at about 3 kpc from the Sun? First, the region is in the Perseus arm. Is there any evidence for strong star formation in that region? Are there any known SN remnants in the region? What about the presence of OB associations? The answer to each of these is "yes." The catalog of Avedisova (2002) shows numerous star-forming regions in that direction. The distances are in general not known, but the molecular cloud data of Yonekura et al. (1997) show several clouds at comparable distances to the Cepheids of this study. The Tycho SN remnant is at $l = 120.^\circ1$ at about 2.4 kpc, somewhat in front of these stars. Another SN remnant is at $l = 116.^\circ9$ at a distance of about 2.7 kpc (Green 2004). There are also a number of well-known OB associations in the direction of $l \approx 120^\circ$ at the proper distance: Cas OB1, Cas OB4, and Cas OB7, among others (Humphreys 1978; Ruprecht et al. 1981). We do *not* imply that the observed SN remnants, OB associations, and molecular clouds currently occupying this volume of the Galaxy are the root cause of the enhancement; we merely point out that the area in which these higher abundance Cepheids are found is a dynamic region with strong star formation, a prime territory for enhancements in elemental abundances.

The amount of processing needed to raise the abundances in the affected region can be roughly estimated. The solar mass fraction of iron is about 1.2×10^{-4}, and at [Fe/H] of +0.2 the mass fraction is about 1.9×10^{-4}. So if there are $10^9\ M_\odot$ of material that we need to process from solar to +0.2, we need to add $7 \times 10^5\ M_\odot$ of iron. Not worrying about SN type, if each event yields $0.5\ M_\odot$ of iron, then we need 1.4×10^6 SNe. Doing this over half of a Galactic rotation (to "guarantee" keeping the region intact) means a rate of 1.4 SNe per 100 yr in the region. This is not absurd. These would be Type II (based on the timescale) with a background of Type Ia SNe. The concentration of Type II SNe could mean that we have an oxygen problem (given that in addition to iron, Type II SNe produce large amounts of oxygen). However, if the stars originally had [O/Fe] less than solar, then the final [O/Fe] could be 0 or less. Note that many solar and slightly greater than solar abundance stars have [O/Fe] < 0 (Luck & Heiter 2006). The stars in the clump have an [O/Fe] ratio of −0.2, which is consistent with other more metal-rich objects, so perhaps the oxygen problem persists. What started the enhancement process? It could be that the region initially had the proper conditions. Another possibility is that a dwarf irregular galaxy hit the region. The impacting gas could have initiated a ministarburst, but the impactor stars would be long gone from the region.

Could the presence of the high-abundance region influence the derived gradients? If it is sufficiently large, and if other parts

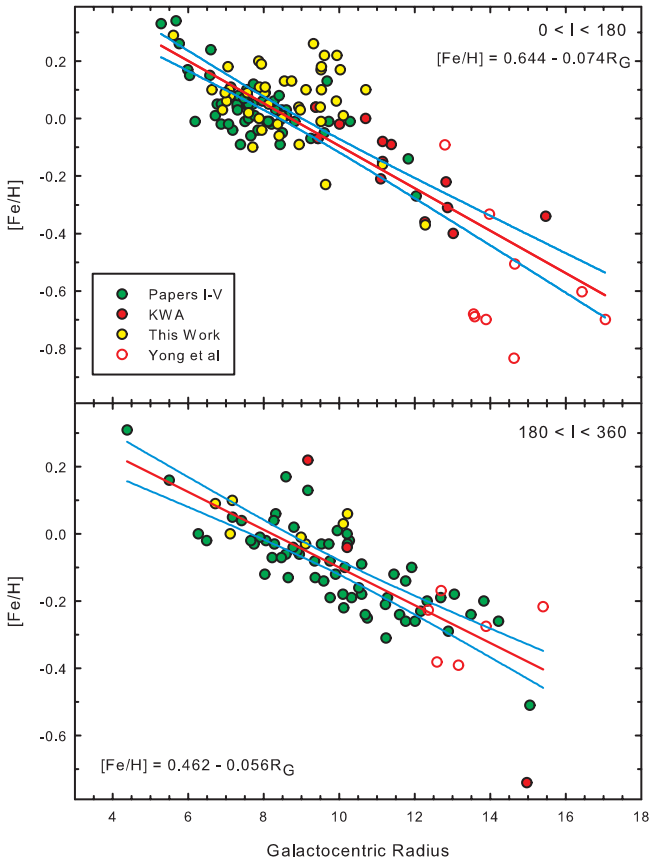

FIG. 13.—[Fe/H] vs. galactocentric distance for the sample Cepheids, divided into two groups based on Galactic longitude. The linear gradients computed from the two sets are given in the figures. The 0°–180° region is significantly influenced by metal-enhanced as well as metal-deficient Cepheids.

of the annulus are not sampled adequately, the answer is obviously yes. Are our gradients perturbed in a major way by the inhomogeneity? To investigate this we have divided our sample into two subsets: those stars within $0^\circ < l < 180^\circ$ and those within $180^\circ < l < 360^\circ$. We show in Figure 13 the gradients in iron from the two subsets. The gradients returned from the two samples are consistent in the sense that both show a strong gradient. However, it is apparent that the gradient on the 0°–180° side is heavily influenced by the stars in the $l = 120^\circ$ region, both the metal-enhanced and the more metal-deficient stars (those from Yong et al. 2006). Note that the most metal-deficient and enhanced stars are limited to a spatial zone in that direction. The 180°–360° zone is much more uniform and yields a gradient much like that given in our previous work. We take the overall Galactic abundance gradient in the present epoch to be about $d[\mathrm{Fe/H}]/dR_G = -0.06$ dex kpc^{-1}, with the caveat that direction matters due to the presence of local inhomogeneities.

In a previous study (Paper V) we expanded on the possibility of the gradient being a nonlinear function with breaks in the overall slope at Galactic radii of about 6.5 and 11 kpc. We interpreted the breaks in the slope as being due to the interaction of the rotation of the spiral arm structure with the rotation of the stellar (and nonstellar) components. Our analysis favors a pattern speed of 20 km s^{-1} kpc^{-1}, which places the inner Lindblad radius at 6.5 kpc and the corotation radius at about 11 kpc. Using simple Galactic chemical evolution models patterned after those of Pagel & Patchett (1975) and Lacey & Fall (1985), we showed that simple modifications of the theory could produce a nonlinear gradient that reproduced the inferred structure in the observed

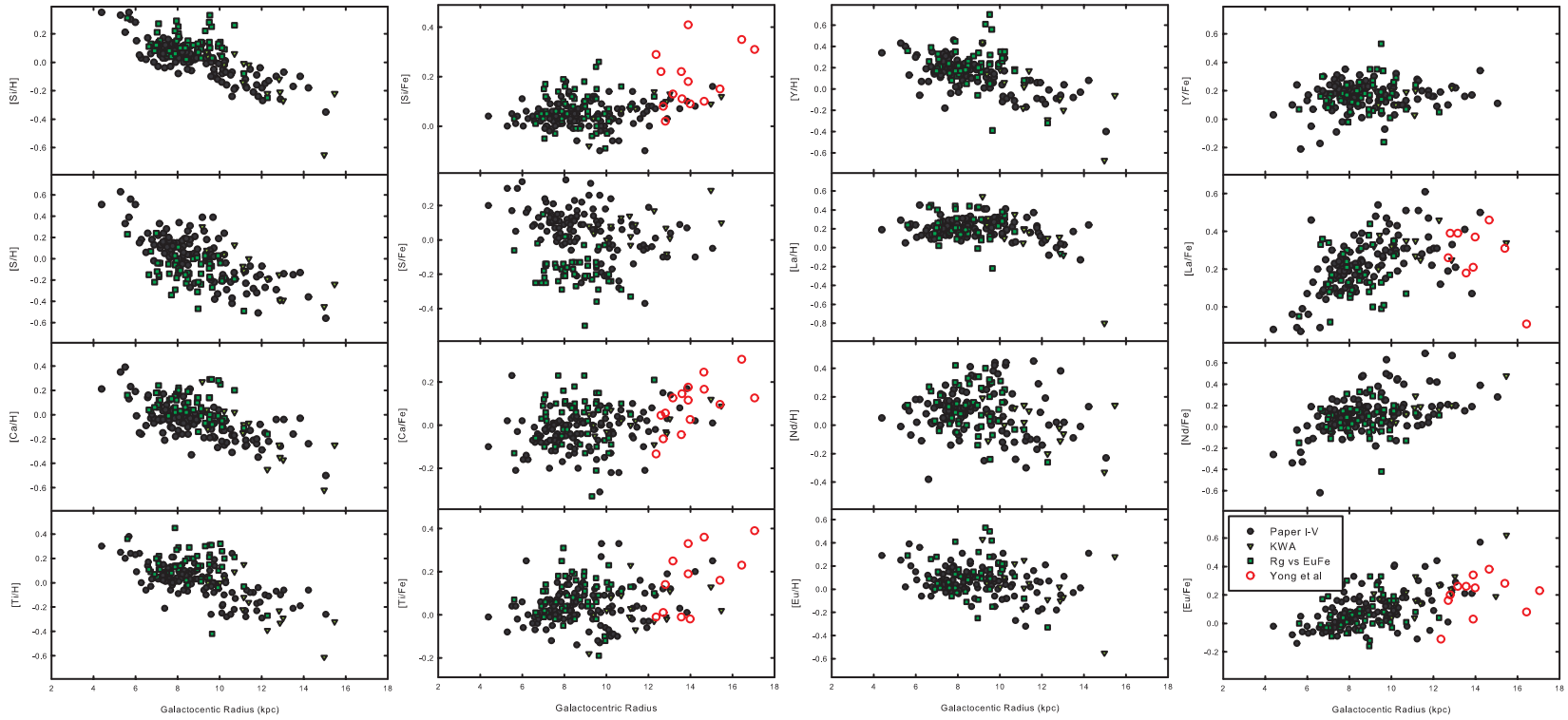

FIG. 14.—Plots of α- (Si, S, Ca, and Ti) and *s*/*r*-process (Y, La, Nd, and Eu) elements in the form [x/H] and [x/Fe] vs. R_G. The light elements show the Galactic abundance gradient prominently. Yttrium shows a distinct gradient, while neodymium shows no evidence for a dependence on galactocentric radius (albeit the scatter is large).

gradient. Does the expanded gradient data set remain consistent with this interpretation? First, with the detection of a local inhomogeneity, a simple 1D model is no longer adequate to explain all features in the metallicity distribution. However, if one smooths over (or suppresses) the local feature, one might be able to recover an underlying global structure.

Examination of Figures 10 and 14 shows that the inflection at 6.5 kpc remains in the gradient data. This inflection is strong (with the caveat that the number of stars is rather small) and well defined in the surface map of the [Fe/H] distribution. We have no doubts about this feature. The break at 10–11 kpc might also be present but is not as pronounced in the total current data set as in the smaller data set previously used. The subset that is most like our previous sample is the $l = 180^\circ$–360° subset (Fig. 13, *bottom*), in which one can see that the outer region abundances are rather consistent (flat out to 14 kpc), with the radial break occurring at about 10–11 kpc. There is some evidence for the 11 kpc break in the total data set (Fig. 8), but the clump of high-abundance stars dilutes/masks the effect. This is especially true in the $l = 0^\circ$–180° subset. If one arbitrarily removes the clump in the total sample, the distribution (in the sense of a linear decline) is rather uniform across the region with $R_G > 6.5$ kpc.

The three stars at the greatest distance from the Galactic center from our work show rather different abundances: $[\mathrm{Fe/H}] = -0.74$, -0.51, and -0.34 for EF Tau, EE Mon, and ER Aur, respectively. The addition of the Yong et al. (2006) data increases the galactocentric radius covered and increases the observed abundance range to about 0.6. The range in R_G for these stars is about 2 kpc (all Cepheids exterior to $R_G = 14.5$ kpc), but the physical separation spans about 15 kpc (see Fig. 11). A typical range in abundance for a span of 2 kpc in galactocentric radius (in zone II especially) is approximately 0.15 dex. Could these stars be indicating that the outer regions of the Galaxy show much more significant variations in abundance than do the regions closer to the solar circle? This would not be especially surprising given the overall lower gas densities and star formation rates that could be significantly influenced by local events.

Our view at the moment is that there exists at least one inflection point in the 1D [Fe/H] distribution (at 6.5 kpc), with the possibility of a second that could correspond in radius to the Galactic corotation point. Given the presence of local inhomogeneities (giant molecular clouds and star-forming regions) and their associated abundance fluctuations, it will be a difficult (but very important) task to sort out local (on the scale of a few kiloparsecs) effects from more global phenomena.

4.2.2. *Other Elements*

Figure 14 shows an array of α- (Si, S, Ca, and Ti) and *s*/*r*-process (Y, La, Nd, and Eu) elements in the form [x/H] and [x/Fe] versus R_G (galactocentric radius). These plots for the α-elements are very similar to our previous work. What is different is that now a gradient in [Y/H] is evident, and there may well be one in [Eu/H]. Only [Nd/H] definitely does not show a gradient, but one must wonder if the large scatter is hiding the actual slope.

We have included the Yong et al. (2006) [x/Fe] data in Figure 14 where available. The data were placed on our abundance scale by comparing their [x/Fe] to ours and offsetting the result as appropriate. Their values typically are larger than ours by 0.1 dex. In the α-elements Si shows three stars with especially high [Si/Fe] ratios and somewhat high [Ca/Fe]. Two of these three stars are the most distant stars present. The [Fe/H] ratios for the most distant two follow the bulk of the data (they are in the $l = 180^\circ$–360° subset). Among the *s*/*r*-process data there is little to distinguish any one star from another at large radius. What is interesting is that the stars interior to $R_G \approx 7$ kpc show a steadily declining [x/Fe] ratio in the *s*/*r*-process data; this is especially evident in the La data. This is due to the iron abundance increasing faster than the heavy elements, indicating the predominance of element production by Type Ia SNe, with heavy-element production by asymptotic giant branch stars lagging behind. The production of *s*/*r*-process elements has been discussed extensively by Burris et al. (2000).

Yong et al. (2006) interpret the somewhat higher α-element presence in their data as indicating that at least some Cepheids in the outer regions of the disk are the result of merger events. They cite as evidence not only the abundance information for Cepheids, but that some of the Cepheids have lower abundances (specifically [Fe/H]) than they observe in outer region open clusters (Yong et al. 2005). Our take on the available data is that it is premature to assign the origin of outer disk Cepheids to a merger origin; the outer disk abundance distribution is still inadequately sampled, and variations in abundance and abundance ratios could very well be due to local inhomogeneities. We are not saying that a merger scenario is impossible—it would certainly lead to local inhomogeneities—only that we feel the state of the current data does not warrant such a leap.

5. SUMMARY

With the newly analyzed Galactic Cepheids (some 50 stars) we have enlarged our homogeneous sample of stars used for Galactic abundance gradient investigation to ~190 objects. The primary results obtained in the present study in conjunction with those reported in our previous work are as follows:

1. The abundance distribution in the Galactic disk shows what is on the whole a linear structure. The Galactic abundance gradient in the present epoch is approximately $d[\mathrm{Fe/H}]/dR_G = -0.06$ dex kpc^{-1}.

2. We have found a localized inhomogeneity in the spatial distribution of the elements. This inhomogeneity lies at about 3 kpc from the Sun in the direction $l \approx 120^\circ$. This region has a mean metallicity about 0.2 dex higher than the solar region.

The next step in this investigation will be twofold: first, we need to further probe the region beyond 3 kpc at $l = 60^\circ$–180°. This will be difficult, as the number of known Cepheids in that region is small, making adequate coverage problematic. Second, the region between $l = 270^\circ$ and 0° is very poorly sampled; this is the Carina area.

We would like to thank Bruce Carney for a number of comments and suggestions that helped improve this paper.

REFERENCES

Allende Prieto, C., Lambert, D. L., & Asplund, M. 2001, ApJ, 556, L63
Andrievsky, S. M., Bersier, D., Kovtyukh, V. V., Luck, R. E., Maciel, W. J., Lépine, J. R. D., & Beletsky, Yu. V. 2002a, A&A, 384, 140 (Paper II)
Andrievsky, S. M., Kovtyukh, V. V., Luck, R. E., Lépine, J. R. D., Maciel, W. J., & Beletsky, Yu. V. 2002b, A&A, 392, 491 (Paper III)
Andrievsky, S. M., Luck, R. E., & Kovtyukh, V. V. 2005, AJ, 130, 1880
Andrievsky, S. M., Luck, R. E., Martin, P., & Lépine, J. R. D. 2004, A&A, 413, 159 (Paper V)
Andrievsky, S. M., et al. 2002c, A&A, 381, 32 (Paper I)
Asplund, M., Grevesse, N., & Sauval, A. J. 2005a, in ASP Conf. Ser. 336, Cosmic Abundances as Records of Stellar Evolution and Nucleosynthesis, ed. T. G. Barnes, III, & F. N. Bash (San Francisco: ASP), 25

Asplund, M., Grevesse, N., Sauval, A. J., Allende Prieto, C., & Blomme, R. 2005b, A&A, 431, 693
Asplund, M., Grevesse, N., Sauval, A. J., Allende Prieto, C., & Kiselman, D. 2004, A&A, 417, 751
Avedisova, V. S. 2002, Astron. Z., 79, 216
Barklem, P. S., Piskunov, N., & O'Mara, B. J. 2000, A&AS, 142, 467
Berdnikov, L. N., & Ignatova, V. V. 2000, in IAU Colloq. 176, The Impact of Large-Scale Surveys on Pulsating Star Research, ed. L. Szabados & D. Kurtz (ASP Conf. Ser. 203; San Francisco: ASP), 244
Berdnikov, L. N., Ignatova, V. V., & Vozyakova, O. V. 1998, Inf. Bull. Variable Stars, 4635, 1
Bravo Alfaro, H., Arellano Ferro, A., & Schuster, W. J. 1997, PASP, 109, 958
Burris, D. L., Pilachowski, C. A., Armandroff, T. E., Sneden, C., Cowan, J. J., & Roe, H. 2000, ApJ, 544, 302
Caputo, F., Marconi, M., Musella, I., & Pont, F. 2001, A&A, 372, 544
de Grijs, R., Kregel, M., & Wesson, K. H. 2001, MNRAS, 324, 1074
Fernie, J. D. 1995, AJ, 110, 2361
Fernie, J. D., Evans, N. R., Beattie, B., & Seager, S. 1995, Inf. Bull. Variable Stars, 4148, 1
Friel, E. D. 1999, Ap&SS, 265, 271
Fry, A. M., & Carney, B. W. 1997, AJ, 113, 1073
Gieren, W. P., Fouqué, P., & Gomez, N. 1998, ApJ, 496, 17
Girardi, L., Bressan, A., Bertelli, G., & Chiosi, C. 2000, A&AS, 141, 371
Green, D. A. 2004, Bull. Astron. Soc. India, 32, 335
Grevesse, N., & Sauval, A. J. 1999, A&A, 347, 348
Gustafsson, B., Bell, R. A., Eriksson, K., & Nordlund, Å. 1975, A&A, 42, 407
Gustafsson, B., Edvardsson, B., Eriksson, K., Mizuno-Wiedner, M., Jørgensen, U. G., & Plez, B. 2002, in ASP Conf. Ser. 288, Stellar Atmosphere Modeling, ed. I. Hubeny, D. Mihalas, & K. Werner (San Francisco: ASP), 331
Heiter, U., & Luck, R. E. 2003, AJ, 126, 2015
Holweger, H. 1974, Sol. Phys., 39, 19
Humphreys, R. M. 1978, ApJS, 38, 309
Iben, I. 1966a, ApJ, 143, 483
———. 1966b, ApJ, 143, 505
———. 1966c, ApJ, 143, 516
Johansson, S., Litzén, U., Lundberg, H., & Zhang, Z. 2003, ApJ, 584, L107
Kiss, L. L., & Szatmary, K. 1998, MNRAS, 300, 616
Kovtyukh, V. V., & Andrievsky, S. M. 1999, A&A, 351, 597
Kovtyukh, V. V., Andrievsky, S. M., Belik, S. I., & Luck, R. E. 2005a, AJ, 129, 433
Kovtyukh, V. V., & Gorlova, N. I. 2000, A&A, 358, 587
Kovtyukh, V. V., Wallerstein, G., & Andrievsky, S. M. 2005b, PASP, 117, 1173 (KWA05)
Lacey, C. G., & Fall, S. M. 1985, ApJ, 290, 154
Laney, C. D., & Stobie, R. S. 1993, MNRAS, 263, 921
López-Corredoira, M., Cabrera-Lavers, A., Garzón, F., & Hammersley, P. L. 2002, A&A, 394, 883
Luck, R. E. 1978, ApJ, 219, 148
Luck, R. E., & Andrievsky, S. M. 2004, AJ, 128, 343
Luck, R. E., Andrievsky, S. M., Kovtyukh, V. V., Korotin, S. A., & Beletsky, Yu. V. 2000, A&A, 361, 189
Luck, R. E., & Bond, H. E. 1989, ApJS, 71, 559
Luck, R. E., Gieren, W. P., Andrievsky, S. M., Kovtyukh, V. V., Fouqué, P., Pont, F., & Kienzle, F. 2003, A&A, 401, 939 (Paper IV)
Luck, R. E., & Heiter, U. 2006, AJ, 131, 3069
Luck, R. E., Kovtyukh, V. V., & Andrievsky, S. M. 2001, A&A, 373, 589
Maciel, W. J., Lago, L. G., & Costa, R. D. D. 2005, A&A, 433, 127
McCarthy, J. K., Sandiford, B. A., Boyd, D., & Booth, J. M. 1993, PASP, 105, 881
McClure-Griffiths, N. M., Dickey, J. M., Gaensler, B. M., & Green, A. J. 2004, ApJ, 607, L127
McNamara, D. H., Madsen, J. B., Barnes, J., & Ericksen, B. F. 2000, PASP, 112, 202
Pagel, B. E. J., & Patchett, B. E. 1975, MNRAS, 172, 13
Phelps, R. 2000, in Chemical Evolution of the Milky Way, ed. F. Matteucci & F. Giovannelli (Dordrecht: Kluwer), 239
Ridgway, S. T., Joyce, R. R., White, N. M., & Wing, R. F. 1980, ApJ, 235, 126
Ruprecht, J., Balázs, B., & White, R. E. 1981, Catalog of Star Clusters and Associations, ed. B. Balázs (Suppl. to 2nd ed.; Budapest: Akad. Kiadó)
Schaller, G., Schaerer, D., Meynet, G., & Maeder, A. 1992, A&AS, 96, 269
Smiljanic, R., Barbuy, B., de Medeiros, J. R., & Maeder, A. 2006, A&A, 449, 655
Sneden, C. 1973, Ph.D. thesis, Univ. Texas, Austin
Szabados, L. 1989, Commun. Konkoly Obs., 94, 1
———. 1991, Commun. Konkoly Obs., 96, 123
Twarog, B. A., Ashman, K. M., & Anthony-Twarog, B. J. 1997, AJ, 114, 2556
Unsöld, A. 1938, Physik der Sternatmosphären, mit besonderer Berücksichtigung der Sonne (Berlin: Springer)
Yonekura, Y., Dobashi, K., Mizuno, A., Ogawa, H., & Fukui, Y. 1997, ApJS, 110, 21
Yong, D., Carney, B. W., & de Almeida, M. L. T. 2005, AJ, 130, 597
Yong, D., Carney, B. W., de Almeida, M. L. T., & Pohl, B. L. 2006, AJ, 131, 2256
Zheng, Z., Flynn, C., Gould, A., Bahcall, J. N., & Salim, S. 2001, ApJ, 555, 393